Supplementary Materials for

On and Off Retinal Circuit Assembly by Divergent Molecular Mechanisms

Lu O. Sun, Zheng Jiang, Michal Rivlin-Etzion, Randal Hand, Colleen M. Brady, Ryota L. Matsuoka, King-Wai Yau, Marla B. Feller, Alex L. Kolodkin*

*Corresponding author. E-mail: kolodkin@jhmi.edu

Published 1 November 2013, *Science* **342**, 1241974 (2013)
DOI: 10.1126/science.1241974

This PDF file includes:

Other Supplementary Material for this manuscript includes the following:
(available at www.sciencemag.org/content/full/342/6158/1241974/suppl/DC1)

Materials and Methods:

Animals. The day of birth in this study is designated as postnatal day 0 (P0). The *PlexA2*-deficient and *Sema6A* gene-trap mouse lines were previously described (*26*). The *PlexA1*$^{-/-}$, *PlexA3*$^{-/-}$, *PlexA4*$^{-/-}$, *Nrp1*$^{Sema-/Sema-}$, *Nrp1*$^{F/F}$, *Nrp2*$^{-/-}$, *Nrp2*$^{F/F}$, *Sema6B*$^{-/-}$, *Sema6C*$^{-/-}$;*Sema6D*$^{-/-}$, and *TRHR-GFP* mice are also described elsewhere(*18, 24, 26-28*). *ROSA*$^{LSL-Tdtomato}$ mouse line was a gift from D. Ginty. *ChAT::cre*, *ChAT::cre*^{ER}, *Six3-cre* and *ROSA*^{iAP} mouse lines were gifts from J. Nathans. *PlexA2*$^{F/+}$ mouse line was generated and directly imported from the European Conditional Mouse Mutagenesis (EUCOMM, Welcome Trust Sanger Institute) (*29*). *PlexA2*$^{F/+}$ mice were genotyped using PCR reactions with two pairs of primers to amplify the *WT* (5'-CATTTCAGGGGATTTTCAGG-3' and 5'- TCTCAGACTCCCTTCACCTCA-3') and the conditional allele (5'- CATTTCAGGGGATTTTCAGG–3' and 5'-TCGTGGTATCGTTATGCGCC-3'). The conditional allele genotype was confirmed using *LacZ* genotyping (5'- ATCACGACGCGCTGTATC-3' and 5'-ACATCGGGCAAATAATATCG-3'). The sizes of the PCR products of *WT*, *PlexA2*^{F}, and *LacZ* are 222bp, 153bp, and 108bp, respectively.

Immunohistochemistry. Eyes were fixed and processed as previously described (*26*). Primary antibodies used in this study include: rabbit anti-PlexA2 (a gift from F. Suto, used at 1:1000), goat anti-mouse Sema6A (Millipore, 1:200), goat anti-choline acetyltransferase (Millipore, 1:100), rabbit anti-Dsred (Clonetech, 1:500), goat anti-vesicular acetylcholine transport (Millipore, 1:500), goat anti-calretinin (Swant, 1:2000), rabbit anti-tyrosine hydroxylase (Millipore, 1:1000), rabbit anti-neurokinin 3 receptor (Calbiochem, 1:3000), mouse anti-

synaptotagmin 2 (ZNP-1, Zebrafish International Resource Center, 1:2000), guinea pig anti-vesicular glutamate transporter type 3 (Millipore, 1:1000), mouse anti-protein kinase C α (Millipore, 1:500), and chicken anti-β galactosidase (Abcam, 1:1000). Confocal fluorescence images were taken using a Zeiss Axioskop2 Mot Plus, LSM 5 Pa confocal microscope.

***In situ* hybridization**. *In situ* hybridization was performed on fresh frozen retina sections (20 μm thickness) using digoxigenin-labeled cRNA probes for *Sema6A* and *PlexA2* as previously described (*17*) (*26*).

Wholemount retina staining. Wholemount retina ICC was performed as previously described (*15*) with a few modifications. Briefly, enucleated eyes were fixed in 4% paraformaldehyde (PFA) for 1 hour at 4°C. The eyecups were dissected out and incubated for 4-5 days at room temperature with primary antibodies in PBS containing 10% donkey serum, 0.5% Triton X-100 and 20% dimethyl sulphoxide (DMSO). Retinas were washed with PBS+0.5% Triton X-100 5 times for 1 hour at room temperature, and then incubated with secondary antibodies in PBS+0.5% Triton X-100 overnight at 4°C. Retinas were washed in PBS+0.5% Triton X-100 5 times for 1 hour at room temperature and then flat mounted. Confocal images were taken using a Zeiss Axioskop2 Mot Plus, LSM 5 Pa confocal microscope or a Zeiss LSM 700 confocal microscope. We did not image the areas near the peripheral edges or the optic nerve head of retinas.

Stripe assay. Stripe assays were performed essentially as previously described (*30*). Retinas obtained from P1-P2 *ChAT::cre; ROSA*$^{LSL\text{-}Tdtomato}$ or *ChAT::cre; ROSA*$^{LSL\text{-}Tdtomato}$*; PlexA2*$^{-/-}$

animals were dissected in cold L-15 (Gibco) and dissociated in 100 μL of digestion buffer containing HBSS (Life Technologies), 2 U/mL papain (Worthington), 2 mM cysteine (Sigma), 0.4 mM EDTA (Sigma) at 37°C for 10 minutes. The digestion was stopped by adding 2 mL of DMEM (Gibco) containing 10% fetal bovine serum at 37°C for 2 minutes. The tissues were dissociated gently using autoclaved Pasteur glass pipette, centrifuged at 1000 rpm for 4 minutes, and then re-suspended in the neurobasal-based culture medium containing 50 units/mL penicillin, 50 μg/mL streptomycin, B-27 supplement, 2 mM L-Glutamine, 10 ng/mL ciliary neurotrophic factor (CNTF, R&D Systems), 50 ng/mL brain-derived neurotrophic factor (BDNF), 5 mM forskolin, 5 μg/mL insulin, 2.5 ng/mL TGF-β1 and TGF-β2 (Peprotech). The re-suspended cells were plated on plates coated with 50μg/ml poly-D-lysine (Sigma), 5 μg/ml laminin (Life Technologies), and alternating stripes (50 μm in width) of 10-20 μg/ mL recombinant Sema6A-Fc (R&D Systems) mixed with Alexa-555-conjugated BSA (10 μg/mL) to allow for fluorescence illumination. Dissociated cells were allowed to grow on the plate with stripes for 5 days in culture medium. The cells were fixed in 4% PFA for 10 minutes and immunostained with antibodies directed against Dsred (Clonetech, 1:1000) and anti-Sema6A (Millipore, 1:500). Neurite lengths of Tdtomato$^+$ cells were measured and quantified using ImageJ plugins.

Density recovery profile (DRP) analysis. DRP analysis and other cell mosaic patterning analyses (including cell density, packing factor, mean distance to nearest neighbor, and regularity index) were performed as previously described (*31*) (*32*).

Alkaline phosphatase (AP) staining. AP staining was performed as previously described (*33*) with minor modifications. Enucleated eyes were fixed in 4% PFA for 1h in 4°C. The retina cups

were dissected out in cold PBS, rinsed 3 times for 10 minutes with HBSS at room temperature and then incubated in a 65°C water bath for 2 hours to inactivate endogenous alkaline phosphatases. After heat inactivation, the retina tissues were rinsed 3 times for 10 min at room temperature with B1 buffer containing 0.1 M Tris (pH7.5) and 0.15 M NaCl. The tissues were then washed 3 times for 10 min with B3 buffer containing 0.1 M Tris (pH9.5) and 0.1 M NaCl, 50 mM $MgCl_2$ and 5 mM levamisole. AP activity was then visualized by incubation with 37.5 g/mL NBT (Roche), 175 g/mL BCIP (Roche) in B3 buffer at room temperature until the AP-generated precipitate appeared.

Targeted SAC dye-filling. 1 μL of 10 ng/μL 4',6-diamidino-2-phenylindole (DAPI) was injected into mouse vitreous 10 hours before single-cell dye injection. SACs were identified by their strong DAPI signals in cell bodies and relatively small soma size (~10μm). Electrodes were pulled from borocilicate glasss capillaries (GC150F-10, Harvard Apparatus). The electrode was tip-filled with 8mM Alexa Flour hydrazide 555 and 0.5% Lucifer Yellow, and back-filled with 3 M KCl. The electrode resistance was 100-180 MΩ. Dye was injected by biphasic current (±1 nA, 2Hz, 3 minutes), and after dye injection, retinas were fixed in 4% PFA over night at 4 °C and washed in PBS 3 times for 45 minutes. The retina tissues were immunostained with anti-ChAT to confirm the identity of dye-filled cells. Images of dye-filled cells were taken using a Zeiss Axioskop2 Mot Plus, LSM 5 Pa confocal microscope and further analyzed using ImageJ plugins.

Sparse Genetic labeling of SACs. Sparse genetic labeling of SACs was performed using two strategies. For P0-P2, we generated and analyzed *ChAT::cre; ROSA*$^{LSL\text{-}Tdtomato}$ mice since we observed sparse and random Tdtomato fluorescence in SACs at these stages with this mouse line.

For later developmental stages, we generated *ChAT::cre^{ER}; ROSA$^{LSL\text{-}Tdtomato}$* and *ChAT::cre^{ER}; ROSA^{iAP}* mice, delivering tamoxifen (Sigma) in a single intraperitoneal injection at P0 (for characterization of P4 retinas) or at P5 (for characterization of animals older than P4) with a dose of 100 µg per animal (*33*). The retinas from these animals were processed and analyzed from P4 to adult.

***Ex vivo* live imaging.** Retina cups were dissected out from enucleated eyes in cold L-15 medium (Gibco) and placed with inner limiting membrane down onto a millicell insert (Millipore). Control and mutant retinas from the same litter were positioned and then cultured in the same millicell insert. The insert was placed onto a 60 mm glass-bottom culture plate (FluoroDish) with the retina culture medium spreading between the glass bottom of the plate and the bottom surface of the insert. The entire culture plate was placed at 37°C, 5% CO_2, to allow for tissue recovery, and was then placed onto the pre-warmed platform of a Zeiss LSM 700 inverted microscope in the humidity chamber (37 °C, 5% CO_2). Time-lapse confocal images were taken at 4-5 different locations in each retina every 20 minutes for 8-12 hours. The images were analyzed using ImageJ plugins.

Recording of light-evoked EPSCs and IPSCs in SACs. Mice with genetically labeled SACs (*ChAT::cre; ROSA$^{LSL\text{-}Tdtomato}$* and *ChAT::cre*; *ROSA$^{LSL\text{-}Tdtomato}$; Sema6A$^{-/-}$*) were dark-adapted for more than 10 hours before experiments were performed. Isolated retinas were superfused with Ames' medium and bubbled with 95% O_2 - 5% CO_2. Patch electrodes (5-7 MΩ) were pulled from borosilicate capillaries (PG10165-4, WPI). The internal solution contained (mM) 120 K-gluconate, 5 NaCl, 4 KCl, 10 HEPES, 2 EGTA, 4 ATP-Mg, 0.3 GTP-NA_2 and 7

Phosphocreatine-Tris. The pH value was adjusted to 7.3 with KOH. SACs, labeled by Tdtomato, were identified by flashes of epifluorescence light. The total exposure time to epifluorescence light before recording was less than 500 ms. Whole-cell patch clamp recording were performed at 25°C, using Multiclamp 700B amplifier. Series resistance of patch electrodes was 10-30 MΩ. Signals were low-pass filtered at 100Hz (8-pole Bessel). White light stimuli were generated by a 100W Xenon lamp. Saturating light intensity (2.8 X 10^{-5} μW/μm^2) was used for all patch-clamp recording experiments. Cells were voltage clamped at -70 mV or 0 mV, to record light-evoked EPSCs or light-evoked IPSCs respectively.

Two-photon targeted loose-patch recording. Two-photon targeted loose-patch recordings of GFP$^+$ cells (*34*) were performed in *TRHR-GFP; Sema6A*$^{+/-}$ and *TRHR-GFP*; *Sema6A*$^{-/-}$ mice of either sex between age P26 and P40. A 60x objective (LUMPlanFl/IR360/0.90 NA water-immersion, Olympus) was used for targeting of GFP$^+$ cells for loose patch recordings. For visual stimulation, we switched to a 20x objective (UMPLFLN/0.50 NA water-immersion, Olympus) that has a broader field of view (775 μm diameter) and allows for stimulation of the cell soma and the surround. Display images were centered on the soma of the recorded cell. We presented four repetitions of drifting bars with positive contrast (bars width = 300 μm; bar length = 1400 μm; velocity = 15 deg/s) in 8 pseudo-randomly chosen directions spaced at 45 degrees intervals, with each trial followed by 500 ms of gray screen. We chose to use relatively long bars and slow speed to facilitate the separation between the On and Off responses (*35*).

For Data analyses we first extracted spike times from these data after offline filtration using a 4 pole Butterworth bandpass filter between 80 and 2000 Hz. Next, we assessed the tuning sharpness of each cell separately for the cell's On and Off responses. The On and Off responses

were separated manually based on a time threshold determined by the experimenter. Following separation, the average spike count in each stimulus direction was normalized by the total number of spikes for all directions. The sum of these normalized responses yielded a vector (On and Off vector sum) whose direction was the preferred direction of the cell, and whose magnitude gave the strength and width of tuning (ranging between 0 and 1: where 0 indicates broad, non-directional, tuning as the cell responds to all directions similarly; and 1 indicates a sharp, directional, tuning as the cell responds only to one single direction). Data analysis was performed in Matlab 7.

Statistical Analysis. Statistical significance of differences between mean values among two or more groups was determined using Student's *t* test or one-way ANOVA analysis followed by Tukey's HSD test, respectively. The criterion for statistical significance was set at $p<0.05$.

SUPPLEMENTARY FIGURES

Fig. S1. *PlexA2* and *Sema6A* mRNA and protein expression in embryonic and early postnatal retinas *in vivo*, and *in vitro* characterization of Sema6A$^+$ and Sema6A$^-$ SAC populations in dissociated retinal cell cultures.

(**A**-**D**) *PlexA2* (A and C) and *Sema6A* (B and D) mRNA expression during embryonic and early postnatal retinal development. *PlexA2* mRNA is not detected at E13.5 (A), but it is upregulated at P0 in the lower region of the outer neuroblastic layer and the upper region of the inner neuroblastic layer (C). *Sema6A* mRNA is expressed in the inner neuroblastic layer during early embryogenesis (B), and its expression persists through P0 with accumulation apparently in the inner neuroblastic layer (D).

(**E**-**H''**) Early postnatal retinas immunostained with anti-PlexA2 (red, E, F, G, and H) and anti-Sema6A (green, E', F', G', and H') reveal complementary protein distributions in the IPL (merged in E'', F'', G'', and H''). Black arrows indicate colocalization of Sema6A immunoreactivity with the inner of the two PlexA2$^+$ IPL stratifications.

(I-**K'')** Dissociated retinal cultures derived from P1 *ChAT::cre; ROSA$^{LSL\text{-}Tdtomato}$* mice, in which SACs are genetically labeled with Tdtomato. SACs in these cultures can be divided into Sema6A$^+$ SACs (cell #1, yellow arrows in I, I', and I'') and Sema6A$^-$ SACs (cell #2, yellow arrowheads in I, I', and I''), similar to On and Off SACs *in vivo*. (J-K'') show magnified views of (I-I'') (J-J'', cell #1; K-K'', cell #2).

Scale bars: 50 μm in (A) for (A)-(D), 20 μm in (H'') for (E)-(H''), 100 μm in (I'') for (I)-(I''), and 10 μm in (K'') for (J)-(K'').

Fig. S2. Generation and characterization of the *PlexA2* conditional allele.

(**A**) Schematic of the targeted *PlexA2* locus (*PlexA2*^{F}). The targeting vector was designed and generated by the EUCOMM resource center as part of the Knockout Mouse Project. The *engrailed 2* splice acceptor (*En2 SA)-IRES-lacZ* cassette is inserted into introns 1 and 2, together with the *neo* gene driven by the *human β-actin* promoter. Exon 1 (ENSMUSE00000350240), which contains part of 5'-UTR and the start of the coding sequence, is flanked by *LoxP* sites. Targeted mice were obtained directly from EUCOMM.

(**B**-**E**) Characterization of *PlexA2*^{F} allele without cre recombinase. *PlexA2*$^{F/-}$ retinas (C) exhibit similar PlexA2 protein expression compared to *PlexA2*$^{+/-}$ retinas (B) (yellow asterisks in B and C). SAC dendritic stratification also appears normal in *PlexA2*$^{F/-}$ retinas. Thus, *PlexA2*^{F} is not a null or hypomorphic allele. n=2 animals for each genotype.

(**F**-**I**) Characterization of β-gal expression in the absence (F) and the presence (G-I) of *Six3-cre*, a pan-retinal cre line. In the absence of the *Six3-cre* allele, β-gal expression is not detected in P14 retina sections (F). In contrast, β-gal is expressed when accompanied by cre expression (G-I). All ChAT^{+} cells are β-gal^{+} (yellow arrowheads in G and H), consistent with PlexA2 protein expression in SACs (Fig. 1). Anti-β-gal immunoreactivity is also detected in ChAT^{+} stratifications (yellow arrows in G), showing that the *PlexA2*^{F} line can be used as a reporter of PlexA2 expression following cre-mediated recombination. We also observed a few non-ChAT^{+} cells that were β-gal-immunopositive cells, suggesting that PlexA2 is transiently expressed in these cells during development. n=2 for each genotype.

(**J**-**M'**) Pan-retinal removal of PlexA2 abolishes PlexA2 protein expression (J and K) and leads to the same SAC stratification phenotypes that are observed in *PlexA2*$^{-/-}$ mutant retinas (compare K' with Fig. 2B). Similarly, removal of PlexA2 protein specifically in SACs greatly attenuates

PlexA2 protein expression (L and M) and generates similar SAC stratification phenotypes (L' and M'). These results show that PlexA2 expressed in SACs is required for segregation of SAC On and Off dendritic stratifications. n=3 animals for each genotype.

Scale bars: 50 μm in (E) for (B)-(E), 20 μm in (F) for (F)-(I), and 50 μm in (M') for (J)-(M').

Fig. S3. Characterization of SAC inner plexiform layer dendritic stratification in *PlexA2*$^{-/-}$ mutants using sparse genetic labeling.

(**A**-**C**) P7 retina section from a *ChAT::cre; ROSA* $^{LSL\text{-}Tdtomato}$ animal immunostained with anti-Dsred (recognizing Tdtomato in A) and anti-ChAT (B). Panel (C) is the merged image of (A) and (B), showing that all ChAT^{+} neurons (both On and Off SACs) express Tdtomato.

(**D**-**F**) Adult retina sections from *ChAT::cre*^{ER}*; ROSA* $^{LSL\text{-}Tdtomato}$*; PlexA2*$^{+/-}$ animals immunostained with anti-Dsred and anti-ChAT. Sparse genetic labeling reveals the dendritic stratifications from single On and Off SACs (schematic shown in panel D). Dendrites from both On and Off SACs stratify in ChAT^{+} sublaminae (white arrows in F). n= 18 SACs from 2 animals.

(**G**-**L**) Characterization of SAC dendritic crossovers in *PlexA2*$^{-/-}$ retinas. Both Off (G-I) and On (J-L) SAC dendrites were found at crossover locations (yellow arrows in H, I, K, and L). Among 35 crossovers that were analyzed in these mutants, dendrites from 17 Off SACs and from 18 On SACs located at the region where the crossovers occurred extended into the On or Off ChAT^{+} laminae, respectively. n=35 SACs from 2 animals.

Scale bars: 50 μm in (C) for (A)-(C), and 50 μm in (K) for (E), (F), (H), (I), (K), and (L).

Fig. S4. Laminar stratification of multiple amacrine cell, ganglion cell, and bipolar cell subtypes in the inner plexiform layer of the *PlexA2*$^{-/-}$ retina is normal.

Adult wild-type and *PlexA2*$^{-/-}$ retinas were immunostained with anti-vesicular acetylcholine transporter (VAChT, labeling SAC dendrites in **A** and **A'**), anti-calretinin (labeling subsets of amacrine and retinal ganglion cells in **B** and **B'**), anti-tyrosine hydroxylase (TH, labeling dopaminergic amacrine cells in **C** and **C'**), anti-neurokinin 3 receptor (NK3R, labeling type 1 and type 2 cone bipolar cells in **D** and **D'**), anti-synaptotagmin2 (Syt2, labeling type 2 and type 6 cone bipolar cells in **E** and **E'**), anti-ChAT (green in **F** and **F'**) and anti-vesicular glutamate transporter type 3 (vGlut3, labeling a subtype of amacrine cells that co-stratify with type 3 and 5 bipolar cells, red in **F** and **F'**), and anti-protein kinase C α (PKCα, labeling rod bipolar cells in **G** and **G'**). Anti-VAChT immunostaining reveals the same SAC stratification defects in *PlexA2*$^{-/-}$ mutants (white arrows in A') as observed using anti-ChAT immunostaining (see Fig. 2B). Subtypes of amacrine cells (B and B', C and C', F and F'), ganglion cells (B and B'), and bipolar cells (D and D', E and E', G and G') exhibit normal sublaminar stratification and axonal targeting in the IPL of *PlexA2*$^{-/-}$ mutants. Note in F and F' that though SACs exhibit dendritic stratification deficits, as revealed by anti-ChAT staining, the overall dendritic stratification of vGlut3^{+} amacrine cells appears normal in *PlexA2*$^{-/-}$ mutants since vGlut3^{+} neurites elaborate processes only between ChAT^{+} On and Off SAC stratifications. n=2 animals.

Scale bar: 50 μm in (G') for (A)-(G').

Fig. S5. Cell body mosaic patterning of On and Off SACs is normal in the *PlexA2*$^{-/-}$ retina.

(**A** and **B**) Wholemount *PlexA2*$^{+/-}$ (A) and *PlexA2*$^{-/-}$ (B) adult retinas stained with anti-ChAT reveal Off SAC cell body mosaic spacing in the inner nuclear layer.

(**C**) Density recovery profile analyses of *PlexA2*$^{+/-}$ (red line) and *PlexA2*$^{-/-}$ (grey line) cell body mosaic spacing. Density recovery profiles of Off SACs do not differ between *PlexA2*$^{+/-}$ and *PlexA2*$^{-/-}$ retinas (n=8 from 2 animals per genotype).

(**D**-**G**) Quantification of Off SAC density (D), packing factor (E), mean distance to nearest neighbor (F), and regularity index (G) shows that PlexA2 plays no role in cell body mosaic spacing of Off SACs. Error bars, S.D.

(**H** and **I**) Wholemount *PlexA2*$^{+/-}$ (H) and *PlexA2*$^{-/-}$ (I) adult retinas stained with anti-ChAT reveal cell body mosaic spacing of On SACs in the ganglion cell layer.

(**J**-**N**) Density recovery profile analyses (J) and quantification of On SAC density (K), packing factor (L), mean distance to nearest neighbor (M), and regularity index (N) show that PlexA2 is not required in regulating cell body mosaic spacing of On SACs (n=8 from 2 animals per genotype). Error bars, S.D.

Scale bar: 50 μm in (I) for (A), (B), (H), and (I).

Fig. S6. SAC dendritic stratification is normal in most *PlexinA* and both *neuropilin*-deficient mice.

Adult retina sections immunostained with anti-ChAT reveal that SAC dendritic stratifications are normal in *PlexA1*$^{-/-}$ (**A**), *PlexA3*$^{-/-}$ (**B**), *PlexA4*$^{-/-}$ (**C**)(*26*), *neuropilin*$^{Sema-/Sema-}$ (*Nrp1*$^{Sema-/Sema-}$) (**D**), *Nrp2*$^{-/-}$ (**E**), and *Six3cre;Nrp1*$^{F/-}$*;Nrp2*$^{F/-}$ (**F**) mutants. On (lower ChAT^{+} stratification) and Off SACs (upper ChAT^{+} stratification) dendritic stratifications are completely segregated and in their appropriate locations in all genotypes listed above (n=3 animals for each genotype).

Scale bar: 50 μm in (F) for (A)-(F).

Fig. S7. Categorization of dye-filled On SAC dendritic morphology and symmetry in *PlexA2*$^{-/-}$ mutants.

(**A-C**) An example of a wild-type On SAC filled with Alexa-555 (A) and double stained with anti-ChAT (B) to confirm the identity of the dye-filled SAC. The cell body of this Alexa-555-filled cell colocalizes with anti-ChAT immunoreactivity (yellow arrows in B and C), showing that it is indeed a SAC. All dye-filled cells in this study were validated as ChAT^{+}.

(**D-G**) Examples of *PlexA2*$^{-/-}$ On SAC dendritic arborization phenotypes of varying severity. These include *PlexA2*$^{-/-}$ SACs missing 1/2 (D), 1/3 (E), 1/4 (F), or none (G) of their dendritic field.

(**H**) Categorization and quantification of dendritic arborization coverage phenotypes observed in wild-type, *PlexA2*$^{-/-}$, *Sema6A*$^{-/-}$, and *PlexA2*$^{-/-}$*;Sema6A*$^{-/-}$ mutants. 80% of On SACs in *PlexA2*$^{-/-}$, Sema6A$^{-/-}$, and *PlexA2*$^{-/-}$*;Sema6A*$^{-/-}$ mutants exhibit loss of 1/4 to 1/2 of their dendritic field, and each category includes a similar fraction of On SACs in *PlexA2*$^{-/-}$, *Sema6A*$^{-/-}$, and *PlexA2*$^{-/-}$*;Sema6A*$^{-/-}$ mutants (n=12 cells from 2 wild-type animals, n=17 from 2 *PlexA2*$^{-/-}$ mutants, n=12 from 2 *Sema6A*$^{-/-}$ mutants, and n=30 from 2 *PlexA2*$^{-/-}$*;Sema6A*$^{-/-}$ mutants).

(**I**) Calculation of a symmetry index based on the fraction of the remaining dendritic field compared to what would be an entire dendritic field. α and β are the angles associated with missing portions of the dendritic field; α and β are subtracted from 360 and then divided by 360 to generate the Symmetry Index used in this study.

Scale bar: 50 μm in (G) for (A)-(G) and (I).

Fig. S8. Defects in dendritic arborization and symmetric organization of On SACs occur early postnatally in *PlexA2*$^{-/-}$ mutant retinas.

(**A**) Representative images of wild-type (left three columns) and *PlexA2*$^{-/-}$ retinas (right three columns) with a genetically encoded SAC reporter at three developmental time points (P0, P2, and P4). On SACs from wild-type retinas exhibit a variety of dendritic morphologies at P0 and P2 (top two rows and left three columns), achieving dendritic symmetry as early as P4 (bottom row and left three columns). On SAC morphology in *PlexA2*$^{-/-}$ mutants (top two rows and right three columns) is indistinguishable from wild-type On SACs at P0 and P2. However, *PlexA2*$^{-/-}$ On SACs fail to establish dendritic symmetry at P4 (bottom row and right three columns). At P4, large gaps between main dendritic branches and tangled dendritic processes are observed in in *PlexA2*$^{-/-}$ On SACs.

(**B** and **C**) Quantification of early postnatal On SAC dendritic field areas (panel B, P0, P2, and P4) and late postnatal On SAC dendritic field area (panel C, P14 and P21) in wild-type and *PlexA2*$^{-/-}$ mutants. No significant difference is observed between wild-type and *PlexA2*$^{-/-}$ mutants at P0 (n=52 SACs for each genotype, p=0.58163 by student's *t* test). However, *PlexA2*$^{-/-}$ mutants start exhibiting mild phenotypes at P2 (n=30 wild-type SACs, n=31 *PlexA2*$^{-/-}$ SACs, *P<0.001 by student's *t* test), and these phenotypes become more severe between P4 and P21 (at P4, n=19 wild-type SACs, n=22 *PlexA2*$^{-/-}$ SACs; at P14, n=16 wild-type SACs, n=10 *PlexA2*$^{-/-}$ SACs; at P21, n=12 wild-type SACs, n=30 *PlexA2*$^{-/-}$ SACs. **P<0.0001 by student's *t* test). Error bars, S.D. Note that the dendritic field area in wild-type increases from 599.9485±108.39 μm^2 at P0 to 30585.19±3595.34 μm^2 at P14, exhibiting a more than 50-fold increase. This dendritic field area increase is accompanied by highly dynamic and rapid outgrowth of the SAC dendrites (see Movie S1).

Scale bars: 20 μm in the most right column of the second row for the first and the second rows in (A), and 20 μm in the most right column of the third row for the third row in (A).

Fig. S9. Sparse genetic labeling of On SACs in *Sema6A*$^{-/-}$ mutants reveals dendritic morphology defects similar to those observed in *PlexA2*$^{-/-}$ mutant retinas, and also allows for detailed Z-projection characterization of *PlexA2*$^{-/-}$ On SACs.

(**A** and **B**) Sparse genetic labeling of On SACs in *Sema6A*$^{+/-}$ (A) and *Sema6A*$^{-/-}$ (B) retinas at P0. Neither control nor *Sema6A*$^{-/-}$ On SACs exhibit symmetrical dendritic organization.

(**C** and **D**) Quantification of the dendritic field area (C) and the symmetry index (D) of On SACs in *Sema6A*$^{+/-}$ and *Sema6A*$^{-/-}$ retinas at P0 (n=52 SACs for each genotype). No significant difference was observed between control and *Sema6A*$^{-/-}$ mutants (for dendritic field area, p=0.13778 by student's *t* test; for symmetry index, p=0.68914 by student's *t* test). Error bars, S.D.

(**E** and **F**) Sparse genetic labeling of On SACs in *Sema6A*$^{+/-}$ (E) and *Sema6A*$^{-/-}$ (F) retinas at P14. *Sema6A*$^{-/-}$ On SACs exhibit loss of a large portion of their dendritic fields (red arrow in F).

(**G** and **H**) Quantification of the dendritic field area (G) and the symmetry index (H) of On SACs in *Sema6A*$^{+/-}$ and *Sema6A*$^{-/-}$ retinas at P14 (n≥16 SACs for each genotype). *Sema6A*$^{-/-}$ On SACs exhibit significantly reduced dendritic field area (panel G, *p<0.0001 by student's *t* test) and significant disruptions in dendritic symmetry (panel H, *p<0.0001 by student's *t* test). Error bars, S.D. Red lines in (D) and (H) represent the mean value of the symmetry index.

Scale bars: 20 μm in (B) for (A) and (B), 50 μm in (F) for (E) and (F).

Fig. S10. The loss of SAC dendritic field coverage and also SAC defects in dendritic morphology observed in the absence of PlexA2 are not correlated with overall SAC position within *PlexA2*$^{-/-}$ retinas.

(**A**-**E**) Representative On SAC images in four quadrants of P14 *PlexA2*$^{+/-}$ retinas (A) are shown in B (position 1, dorsal), C (position 2, temporal), D (position 3, ventral), and E (position 4, nasal). *PlexA2*$^{+/-}$ SACs exhibit radially-symmetric dendritic morphology in all positions.

(**F-J**) *En face* view of a flat-mounted P14 *PlexA2*$^{-/-}$ retina with sparse genetically labeled SACs. A range of On SAC dendritic-symmetry defects was found in all four quadrants of this retina, and no correlation of SAC dendritic phenotypes with cell body position within the retina was observed (G-J, red arrows). Note in (G), (I), and (J), that *PlexA2*$^{-/-}$ On SACs exhibit a dendritic field loss in multiple directions. n=2 animals for both genotypes. Scale bars, 2000 μm in (F) for (A) and (F), 50 μm in (J) for (B)-(E) and (G)-(J).

Fig. S11. Dendritic stratification and arborization phenotypes are not correlated in *PlexA2*$^{-/-}$ mutants.

(**A**-**C**) *En face* projection images of *PlexA2*$^{+/-}$ (A) and *PlexA2*$^{-/-}$ On SACs (B and C).

(**A'-C''**) Rotated stacked images show cross-sectional views of the same On SACs shown in (A), (B), and (C). *PlexA2*$^{+/-}$ On SACs exhibit normal dendritic stratification (A', schematics shown in A'', n=10 On SACs). In contrast, two types of On SACs were observed in *PlexA2*$^{-/-}$ mutants: those with normal dendritic stratification (B' and B'', n=11 On SACs), and those with disrupted dendritic stratification (red arrows in C' and C'', n=18 On SACs). Note that the On SAC in (B) exhibits many self-crossings along distal dendritic processes (red rectangle in B), however these dendrites still stratify within their proper sublamina (red arrowhead in B').

(**D** and **D'**) *En face* projection images of genetically labeled On SACs in *PlexA2*$^{+/-}$ (D) and *PlexA2*$^{-/-}$ retinas (D'). *PlexA2*$^{+/-}$ On SACs exhibit stereotypic symmetrical morphology (D), whereas *PlexA2*$^{-/-}$ On SACs lack a large portion of their dendritic fields (red arrow in D**'**).

(**E-F'**) Rotated stacked images to show cross-sectional views of the same On SACs in (D) and (D'). Despite lacking a large portion of their dendritic fields (red arrow in D'), *PlexA2*$^{-/-}$ On SACs exhibit normal dendritic stratification in the portion of the dendritic field that includes massive coverage area loss (yellow arrowhead in E', also see Movie S3). This strongly suggests that dendritic arborization phenotypes and stratification phenotypes are not correlated.

(**G**) All *PlexA2*$^{+/-}$ On SAC dendrites stratify in the ChAT^{+} On sublaminae, and pooled symmetry indices are close to 1 (n=10 *PlexA2*$^{+/-}$ On SACs). In contrast, dendritic-field asymmetry in *PlexA2*$^{-/-}$ On SACs is the same in On SACs that restrict their dendrites to the correct On SAC sublamina (middle column of plot, n=11 *PlexA2*$^{-/-}$ On SACs) and in SACs that extend their dendrites into regions with an aberrant cholinergic plexus between the two normal ChAT^{+} sublaminae ('crossovers'; right column, n=18 *PlexA2*$^{-/-}$ On SACs).

(**H**) All *PlexA2*$^{+/-}$ Off SAC dendrites stratify in the ChAT^{+} Off sublaminae, and pooled symmetry indices are close to 1 (n=15 *PlexA2*$^{+/-}$ Off SACs). In *PlexA2*$^{-/-}$ mutants, Off SACs retain normal dendritic field symmetry no matter where they stratify their dendrites (n=21 *PlexA2*$^{-/-}$ Off SACs in which stratification occurs in a region that does not include a crossover; n=15 *PlexA2*$^{-/-}$ Off SACs that stratify in a region that includes a dendritic process crossover). Taken together, these data indicate that the defects we observe in SAC dendritic arborization are not correlated with stratification crossovers.

Scale bar: 50 μm in (A) for (A)-(C'), 50 μm in (D') for (D)-(F').

Fig. S12. Off SACs in *PlexA2*$^{-/-}$ mutant retinas exhibit normal dendritic arborization and plexus organization.

(**A-F'**) Sparse genetic labeling of On (A' and D') and Off (A and D) SACs coupled with anti-ChAT immunostaining of On (B' and E') and Off (B and E) SAC dendritic plexuses in wild-type (A-C') and *PlexA2*$^{-/-}$ (D-F') retinas. On and Off SACs in wild-type retinas exhibit stereotypic symmetrical morphology (A and A'). In contrast, overall dendritic organization of *PlexA2*$^{-/-}$ On SACs is disrupted (red arrow in D'). However, *PlexA2*$^{-/-}$ Off SACs display normal dendritic morphology (D). Similarly, SAC plexus organization revealed by anti-ChAT immunostaining shows that only *PlexA2*$^{-/-}$ On SAC plexuses are compromised, as indicated by large gaps and holes (yellow arrowheads in E' and F'). These results also argue against SAC dendritic elaboration phenotypes being associated with dendritic stratification phenotypes.

(**G**) Quantification of average SAC plexus gap areas in P11 wild-type, *Sema6A*$^{-/-}$, and *PlexA2*$^{-/-}$ retinas. Both *Sema6A*$^{-/-}$ and *PlexA2*$^{-/-}$ mutants exhibit increased gap areas in the On SAC plexus, but not in the Off SAC plexus, as compared to wild-type. n≥17 for each genotype analyzed. Error bars, S.E.M. *p<0.0001.

Scale bar: 100 μm in (H) for (A)-(H).

Fig. S13. The *ROSA*^{iAP} reporter expressed in *PlexA2*$^{-/-}$ SACs also reveals dendritic arborization and symmetry defects of On SACs.

(**A** and **B**) Representative images of On SACs in wild-type (A) and *PlexA2*$^{-/-}$ mutants (B) genetically labeled with an alkaline phosphatase (AP) reporter. Dark purple in (A) and (B) results from the AP catalyzed reaction product. Note that the wild-type On SAC has symmetric

dendritic organization at P5 (A), whereas the dendrites of the P5 *PlexA2*$^{-/-}$ On SACs are tangled together and fail to elaborate a symmetric arbor (B, red arrowheads).

(**C** and **D**) Quantification of P5 wild-type and *PlexA2*$^{-/-}$ On SAC dendritic field area (C) and symmetry index (D). Error bars, S.D. n≥39 SACs for each genotype. *p<0.0001 by student's *t* test. Red lines in (D) represent the mean value of symmetry index.

(**E-G'**) Representative images of Off (E-G) and On (E'-G') SACs in P14 wild-type (E and E'), *PlexA2*$^{+/-}$ (F and F'), and *PlexA2*$^{-/-}$ (G and G') retinas. No morphological difference was observed between wild-type and *PlexA2*$^{+/-}$ On and Off SACs. In contrast, On SAC in *PlexA2*$^{-/-}$ mutants exhibit greatly disrupted morphology (red arrows in G'), whereas the overall morphology of Off SACs in *PlexA2*$^{-/-}$ mutants appears normal (G).

(**H** and **I**) Quantification of dendritic field area (H) and symmetry index (I) of On and Off SACs in P14 wild-type, *PlexA2*$^{+/-}$, and *PlexA2*$^{-/-}$ retinas (n≥10 SACs for each genotype). No significant difference was found between wild-type and *PlexA2*$^{+/-}$ retinas with respect to On and Off SAC dendritic field areas (for On SACs, p=0.79122 by student's *t* test; for Off SACs, p=0.19512 by student's *t* test). However, *PlexA2*$^{-/-}$ SACs exhibit reduced dendritic field area for both On and Off SACs, in comparison to wild-type SACs (for On SACs, **p<0.0001 by student's *t* test; for Off SACs, *p<0.001 by student's *t* test). Off SACs from wild-type, *PlexA2*$^{+/-}$, and *PlexA2*$^{-/-}$ retinas exhibit symmetric morphology, whereas the dendritic symmetry is disrupted only in *PlexA2*$^{-/-}$ On SACs (I). Error bars, S.D. Red lines in (I) represent mean values of the symmetry index.

Scale bars: 20 μm in (B) for (A) and (B), 100 μm in (E') for (E)-(G').

Fig. S14. Conditional removal of PlexA2 in SACs does not disrupt Off SAC dendritic plexus organization, and Sema6B, 6C, and 6D are not required for On or Off SAC dendritic plexus organization.

(**A**) Dendritic plexus organization of Off SACs in control (left) and *ChAT::cre; PlexA2*$^{F/-}$ (right) retinas. Conditional removal of PlexA2 protein in SACs does not disrupt Off SAC plexus organization.

(**B**) Quantification of On and Off SAC plexus gap areas in control and *ChAT::cre; PlexA2*$^{F/-}$ retinas. *ChAT::cre; PlexA2*$^{F/-}$ animals exhibit increased gap areas in the On SAC plexus, but normal gap areas in the Off SAC plexus as compared to control animals. Together with results in Fig. 4I, these observations show that PlexA2 is cell-type autonomously required for On, but not Off, SAC dendritic plexus organization. n≥6 for both genotypes examined. Error bars, S.E.M. *p<0.0001 by student's *t* test.

(**C**) Flat-mount views of Off (top panels) and On SAC (bottom panels) dendritic plexuses in P21 wild-type, *Sema6A*$^{-/-}$, *Sema6B*$^{-/-}$, and *Sema6C*$^{-/-}$*;Sema6D*$^{-/-}$ mutant retinas, labeled using anti-ChAT immunostaining. Only the On SAC dendritic plexus in *Sema6A*$^{-/-}$ mutants exhibits large gaps and holes (indicated by yellow asterisks). The other genotypes show normal ChAT^{+} plexus organization. n=3 animals for each genotype.

(**D**) Quantification of average gap areas of On and Off SAC plexus in P21 wild-type, *Sema6A*$^{-/-}$, *Sema6B*$^{-/-}$, and *Sema6C*$^{-/-}$*;6D*$^{-/-}$ retinas. *Sema6A*$^{-/-}$ mutants exhibit increased On SAC plexus gap areas, but normal Off SAC plexus gap areas, as compared to wild-type. In contrast, *Sema6B*$^{-/-}$ and *Sema6C*$^{-/-}$*;6D*$^{-/-}$ mutants exhibit indistinguishable On and Off SAC plexus gap areas as compared to wild-type. n≥6 for each genotype analyzed. Error bars, S.E.M. *p<0.0001.

Scale bar: 100 μm in the right panel of (A) for (A) and (C).

Fig. S15. *Sema6A*$^{-/-}$ mutants exhibit aberrant GABAergic light-evoked IPSCs.

(**A**-**B'**) Representative light-evoked IPSC traces from wild-type (A and A') and *Sema6A*$^{-/-}$ (B and B') On SACs (voltage-clamped at 0mV for all experiments). Panels A' and B' show the onset of light-evoked IPSC traces (from A and B, respectively) with expanded time scales. The amplitude of wild-type light-evoked IPSCs does not exceed 100 pA (A and A'), whereas *Sema6A*$^{-/-}$ mutants exhibit a large (over 300 pA) light-evoked IPSC (red arrows in B and B' point to the aberrant current).

(**C**) Quantification of the amplitude of the light evoked-IPSCs in wild-type (n=4 On SACs) and *Sema6A*$^{-/-}$ retinas (n=5 On SACs). Error bars, S.E.M. *p=0.04319 by student's *t* test.

(**D**) Recordings from *Sema6A*$^{-/-}$ On SACs show that the aberrant IPSCs observed at the onset of light stimulus are completely blocked by 100 μM PTX (picrotoxin, an antagonist of both $GABA_A$ and $GABA_C$ receptors, n=4, top panel). These currents are partially recovered following washout (n=3, bottom panel). Light stimulations for all experiments were a full field, saturating intensity, white light from a Xenon lamp.

Fig. S16. *TRHR-GFP; Sema6A*$^{-/-}$ direction-selective ganglion cell dendrites cofasciculate with On and Off SAC dendrites.

Alexa-555 dye-filling individual *TRHR-GFP; Sema6A*$^{+/-}$ direction-selective ganglion cell**s** (**A** and **C**) and *TRHR-GFP; Sema6A*$^{-/-}$ direction-selective ganglion cells (**F** and **H**), coupled with anti-VAChT immunostaining (**B**, **B'**, **D**, **D'**, **G**, **G'**, **I**, and **I'**). *TRHR-GFP; Sema6A*$^{+/-}$ direction-selective ganglion cells bistratify with Off (B and B') and On (D and D') SAC dendritic plexuses. Although the On SAC dendritic plexus is disrupted in *Sema6A*$^{-/-}$ mutants (compare D and I),

TRHR-GFP; Sema6A$^{-/-}$ direction-selective ganglion cells still co-fasciculate with both Off (G and G') and On (I and I') SAC dendritic plexuses. (**E** and **J**) Z-stack projections of both On and Off THRH-GFP^{+} dendrites from a single On-Off DSGC in *Sema6A*$^{+/-}$ and *Sema6A*$^{-/-}$ retinas.
Scale bars: 100 μm in (I) for (A)-(J), 25 μm in (I') for (B'), (G'), (D'), and (I').

Fig. S17. *TRHR-GFP; Sema6A*$^{-/-}$ On-Off direction-selective ganglion cells exhibit similar On and Off dendritic field areas as observed in *TRHR-GFP; Sema6A*$^{+/-}$ mice.

(**A**) Representative images of Alexa-555 dye-filled *TRHR-GFP; Sema6A*$^{+/-}$ direction-selective ganglion cells (left three columns) and *TRHR-GFP; Sema6A*$^{-/-}$ direction-selective ganglion cells (right three columns). The three rows (from top to bottom) show (1) the Off plexus, (2) the On plexus, and (3) complete Z-projection (On and Off plexus) of individual TRHR-GFP^{+} On-Off direction-selective ganglion cells.

(**B**) Quantification of Off and On dendritic field areas of TRHR-GFP^{+} On-Off direction-selective ganglion cells. *TRHR-GFP; Sema6A*$^{-/-}$ direction-selective ganglion cells do not exhibit significantly altered dendritic field areas, as compared to *TRHR-GFP; Sema6A*$^{+/-}$ direction-selective ganglion cells (n=15 TRHR-GFP^{+} direction-selective ganglion cells from 2 animals for both genotypes. For Off dendritic field areas, p=0.27; for On dendritic field areas, p=0.08. Statistical analyses were performed using Students' *t* test.). Error bars, S.E.M.
Scale bar: 100 μm.

Supplementary Movies:

Movies S1 and **S2:** *Ex vivo* live imaging of On SACs from *ChAT::cre; ROSA* $^{LSL\text{-}Tdtomato}$ (Movie S1) and *ChAT::cre; ROSA* $^{LSL\text{-}Tdtomato}$*; PlexA2*$^{-/-}$ (Movie S2) retinas at P1 (12 hrs. total live imaging, with one image every 20min).

Movie S3: Dendritic stratification and arborization phenotypes are not correlated in *PlexA2*$^{-/-}$ mutants (Z-stack of P21 *PlexA2*$^{+/-}$ and *PlexA2*$^{-/-}$ retinas with sparse SAC genetic labeling, followed by rotation to reveal the Z-plane SAC stratification in the inner plexiform layer).

Movie S4: *En face* views of genetically labeled On and Off SACs in *Sema6A*$^{+/-}$ and *Sema6A*$^{-/-}$ retinas (Z-stack of P11 retinas, starting from the ganglion cell layer to the inner nuclear layer).

Movie S5: *En face* view (from Off plexus to the inner nuclear layer) of genetically labeled Off SACs in a P14 *PlexA2*$^{+/-}$ retina, followed by Z-stack projection of the same Off SAC to show its X-Y-plane morphology, and then a rotation to reveal dendritic stratification in the inner plexiform layer. Yellow arrow indicates dendritic stratification in the Off plexus.

Movie S6: *En face* view (from Off plexus to the inner nuclear layer) of genetically labeled Off SACs in a P14 *PlexA2*$^{-/-}$ retina, followed by Z-stack projection of the same Off SAC to show its X-Y-plane morphology, and then a rotation to reveal dendritic stratification in the inner plexiform layer. Yellow arrow (in the Z plane) indicates normal dendritic stratification in the Off

plexus, and yellow arrowheads (in the X-Y plane and the Z plane) show the mis-stratified dendritic processes in the On plexus.

References

1. J. B. Demb, Cellular mechanisms for direction selectivity in the retina. *Neuron* **55**, 179–186 (2007). doi:10.1016/j.neuron.2007.07.001 Medline

2. W. Wei, M. B. Feller, Organization and development of direction-selective circuits in the retina. *Trends Neurosci.* **34**, 638–645 (2011). doi:10.1016/j.tins.2011.08.002 Medline

3. D. I. Vaney, B. Sivyer, W. R. Taylor, Direction selectivity in the retina: Symmetry and asymmetry in structure and function. *Nat. Rev. Neurosci.* **13**, 194–208 (2012). Medline

4. R. H. Masland, The neuronal organization of the retina. *Neuron* **76**, 266–280 (2012). doi:10.1016/j.neuron.2012.10.002 Medline

5. L. M. Chalupa, E. Günhan, Development of On and Off retinal pathways and retinogeniculate projections. *Prog. Retin. Eye Res.* **23**, 31–51 (2004). doi:10.1016/j.preteyeres.2003.10.001 Medline

6. R. C. Stacy, R. O. L. Wong, Developmental relationship between cholinergic amacrine cell processes and ganglion cell dendrites of the mouse retina. *J. Comp. Neurol.* **456**, 154–166 (2003). doi:10.1002/cne.10509 Medline

7. A. D. Huberman, W. Wei, J. Elstrott, B. K. Stafford, M. B. Feller, B. A. Barres, Genetic identification of an On-Off direction-selective retinal ganglion cell subtype reveals a layer-specific subcortical map of posterior motion. *Neuron* **62**, 327–334 (2009). doi:10.1016/j.neuron.2009.04.014 Medline

8. J. N. Kay, I. De la Huerta, I. J. Kim, Y. Zhang, M. Yamagata, M. W. Chu, M. Meister, J. R. Sanes, Retinal ganglion cells with distinct directional preferences differ in molecular identity, structure, and central projections. *J. Neurosci.* **31**, 7753–7762 (2011). doi:10.1523/JNEUROSCI.0907-11.2011 Medline

9. T. Euler, P. B. Detwiler, W. Denk, Directionally selective calcium signals in dendrites of starburst amacrine cells. *Nature* **418**, 845–852 (2002). doi:10.1038/nature00931 Medline

10. K. L. Briggman, M. Helmstaedter, W. Denk, Wiring specificity in the direction-selectivity circuit of the retina. *Nature* **471**, 183–188 (2011). doi:10.1038/nature09818 Medline

11. W. Wei, A. M. Hamby, K. Zhou, M. B. Feller, Development of asymmetric inhibition underlying direction selectivity in the retina. *Nature* **469**, 402–406 (2011). doi:10.1038/nature09600 Medline

12. K. Yonehara, K. Balint, M. Noda, G. Nagel, E. Bamberg, B. Roska, Spatially asymmetric reorganization of inhibition establishes a motion-sensitive circuit. *Nature* **469**, 407–410 (2011). doi:10.1038/nature09711 Medline

13. J. L. Lefebvre, D. Kostadinov, W. V. Chen, T. Maniatis, J. R. Sanes, Protocadherins mediate dendritic self-avoidance in the mammalian nervous system. *Nature* **488**, 517–521 (2012). doi:10.1038/nature11305 Medline

14. R. L. Matsuoka, O. Chivatakarn, T. C. Badea, I. S. Samuels, H. Cahill, K. Katayama, S. R. Kumar, F. Suto, A. Chédotal, N. S. Peachey, J. Nathans, Y. Yoshida, R. J. Giger, A. L. Kolodkin, Class 5 transmembrane semaphorins control selective mammalian retinal

lamination and function. *Neuron* **71**, 460–473 (2011). doi:10.1016/j.neuron.2011.06.009 Medline

15. R. L. Matsuoka, Z. Jiang, I. S. Samuels, K. T. Nguyen-Ba-Charvet, L. O. Sun, N. S. Peachey, A. Chédotal, K. W. Yau, A. L. Kolodkin, Guidance-cue control of horizontal cell morphology, lamination, and synapse formation in the mammalian outer retina. *J. Neurosci.* **32**, 6859–6868 (2012). doi:10.1523/JNEUROSCI.0267-12.2012 Medline

16. F. Suto, M. Tsuboi, H. Kamiya, H. Mizuno, Y. Kiyama, S. Komai, M. Shimizu, M. Sanbo, T. Yagi, Y. Hiromi, A. Chédotal, K. J. Mitchell, T. Manabe, H. Fujisawa, Interactions between plexin-A2, plexin-A4, and semaphorin 6A control lamina-restricted projection of hippocampal mossy fibers. *Neuron* **53**, 535–547 (2007). doi:10.1016/j.neuron.2007.01.028 Medline

17. J. Renaud, G. Kerjan, I. Sumita, Y. Zagar, V. Georget, D. Kim, C. Fouquet, K. Suda, M. Sanbo, F. Suto, S. L. Ackerman, K. J. Mitchell, H. Fujisawa, A. Chédotal, Plexin-A2 and its ligand, Sema6A, control nucleus-centrosome coupling in migrating granule cells. *Nat. Neurosci.* **11**, 440–449 (2008). doi:10.1038/nn2064 Medline

18. R. L. Matsuoka, L. O. Sun, K. Katayama, Y. Yoshida, A. L. Kolodkin, Sema6B, Sema6C, and Sema6D expression and function during mammalian retinal development. *PLoS ONE* **8**, e63207 (2013). doi:10.1371/journal.pone.0063207 Medline

19. K. J. Ford, M. B. Feller, Assembly and disassembly of a retinal cholinergic network. *Vis. Neurosci.* **29**, 61–71 (2012). doi:10.1017/S0952523811000216 Medline

20. R. O. Wong, S. P. Collin, Dendritic maturation of displaced putative cholinergic amacrine cells in the rabbit retina. *J. Comp. Neurol.* **287**, 164–178 (1989). doi:10.1002/cne.902870203 Medline

21. J. L. Lefebvre, Y. Zhang, M. Meister, X. Wang, J. R. Sanes, Gamma-Protocadherins regulate neuronal survival but are dispensable for circuit formation in retina. *Development* **135**, 4141–4151 (2008). doi:10.1242/dev.027912 Medline

22. B. N. Peters, R. H. Masland, Responses to light of starburst amacrine cells. *J. Neurophysiol.* **75**, 469–480 (1996). Medline

23. K. Yoshida, D. Watanabe, H. Ishikane, M. Tachibana, I. Pastan, S. Nakanishi, A key role of starburst amacrine cells in originating retinal directional selectivity and optokinetic eye movement. *Neuron* **30**, 771–780 (2001). doi:10.1016/S0896-6273(01)00316-6 Medline

24. M. Rivlin-Etzion, K. Zhou, W. Wei, J. Elstrott, P. L. Nguyen, B. A. Barres, A. D. Huberman, M. B. Feller, Transgenic mice reveal unexpected diversity of on-off direction-selective retinal ganglion cell subtypes and brain structures involved in motion processing. *J. Neurosci.* **31**, 8760–8769 (2011). doi:10.1523/JNEUROSCI.0564-11.2011 Medline

25. L. Haklai-Topper, G. Mlechkovich, D. Savariego, I. Gokhman, A. Yaron, Cis interaction between Semaphorin6A and Plexin-A4 modulates the repulsive response to Sema6A. *EMBO J.* **29**, 2635–2645 (2010). doi:10.1038/emboj.2010.147 Medline

26. R. L. Matsuoka, K. T. Nguyen-Ba-Charvet, A. Parray, T. C. Badea, A. Chédotal, A. L. Kolodkin, Transmembrane semaphorin signalling controls laminar stratification in the mammalian retina. *Nature* **470**, 259–263 (2011). doi:10.1038/nature09675 Medline

27. A. Walz, I. Rodriguez, P. Mombaerts, Aberrant sensory innervation of the olfactory bulb in neuropilin-2 mutant mice. *J. Neurosci.* **22**, 4025–4035 (2002). Medline

28. C. Gu, E. R. Rodriguez, D. V. Reimert, T. Shu, B. Fritzsch, L. J. Richards, A. L. Kolodkin, D. D. Ginty, Neuropilin-1 conveys semaphorin and VEGF signaling during neural and cardiovascular development. *Dev. Cell* **5**, 45–57 (2003). doi:10.1016/S1534-5807(03)00169-2 Medline

29. W. C. Skarnes, B. Rosen, A. P. West, M. Koutsourakis, W. Bushell, V. Iyer, A. O. Mujica, M. Thomas, J. Harrow, T. Cox, D. Jackson, J. Severin, P. Biggs, J. Fu, M. Nefedov, P. J. de Jong, A. F. Stewart, A. Bradley, A conditional knockout resource for the genome-wide study of mouse gene function. *Nature* **474**, 337–342 (2011). doi:10.1038/nature10163 Medline

30. M. M. Riccomagno, A. Hurtado, H. Wang, J. G. Macopson, E. M. Griner, A. Betz, N. Brose, M. G. Kazanietz, A. L. Kolodkin, The RacGAP β2-Chimaerin selectively mediates axonal pruning in the hippocampus. *Cell* **149**, 1594–1606 (2012). doi:10.1016/j.cell.2012.05.018 Medline

31. J. N. Kay, M. W. Chu, J. R. Sanes, MEGF10 and MEGF11 mediate homotypic interactions required for mosaic spacing of retinal neurons. *Nature* **483**, 465–469 (2012). doi:10.1038/nature10877 Medline

32. S. K. Chen, K. S. Chew, D. S. McNeill, P. W. Keeley, J. L. Ecker, B. Q. Mao, J. Pahlberg, B. Kim, S. C. Lee, M. A. Fox, W. Guido, K. Y. Wong, A. P. Sampath, B. E. Reese, R. Kuruvilla, S. Hattar, Apoptosis regulates ipRGC spacing necessary for rods and cones to drive circadian photoentrainment. *Neuron* **77**, 503–515 (2013). doi:10.1016/j.neuron.2012.11.028 Medline

33. T. C. Badea, Z. L. Hua, P. M. Smallwood, J. Williams, T. Rotolo, X. Ye, J. Nathans, New mouse lines for the analysis of neuronal morphology using CreER(T)/loxP-directed sparse labeling. *PLoS ONE* **4**, e7859 (2009). doi:10.1371/journal.pone.0007859 Medline

34. W. Wei, J. Elstrott, M. B. Feller, Two-photon targeted recording of GFP-expressing neurons for light responses and live-cell imaging in the mouse retina. *Nat. Protoc.* **5**, 1347–1352 (2010). doi:10.1038/nprot.2010.106 Medline

35. S. Weng, W. Sun, S. He, Identification of ON-OFF direction-selective ganglion cells in the mouse retina. *J. Physiol.* **562**, 915–923 (2005). doi:10.1113/jphysiol.2004.076695 Medline

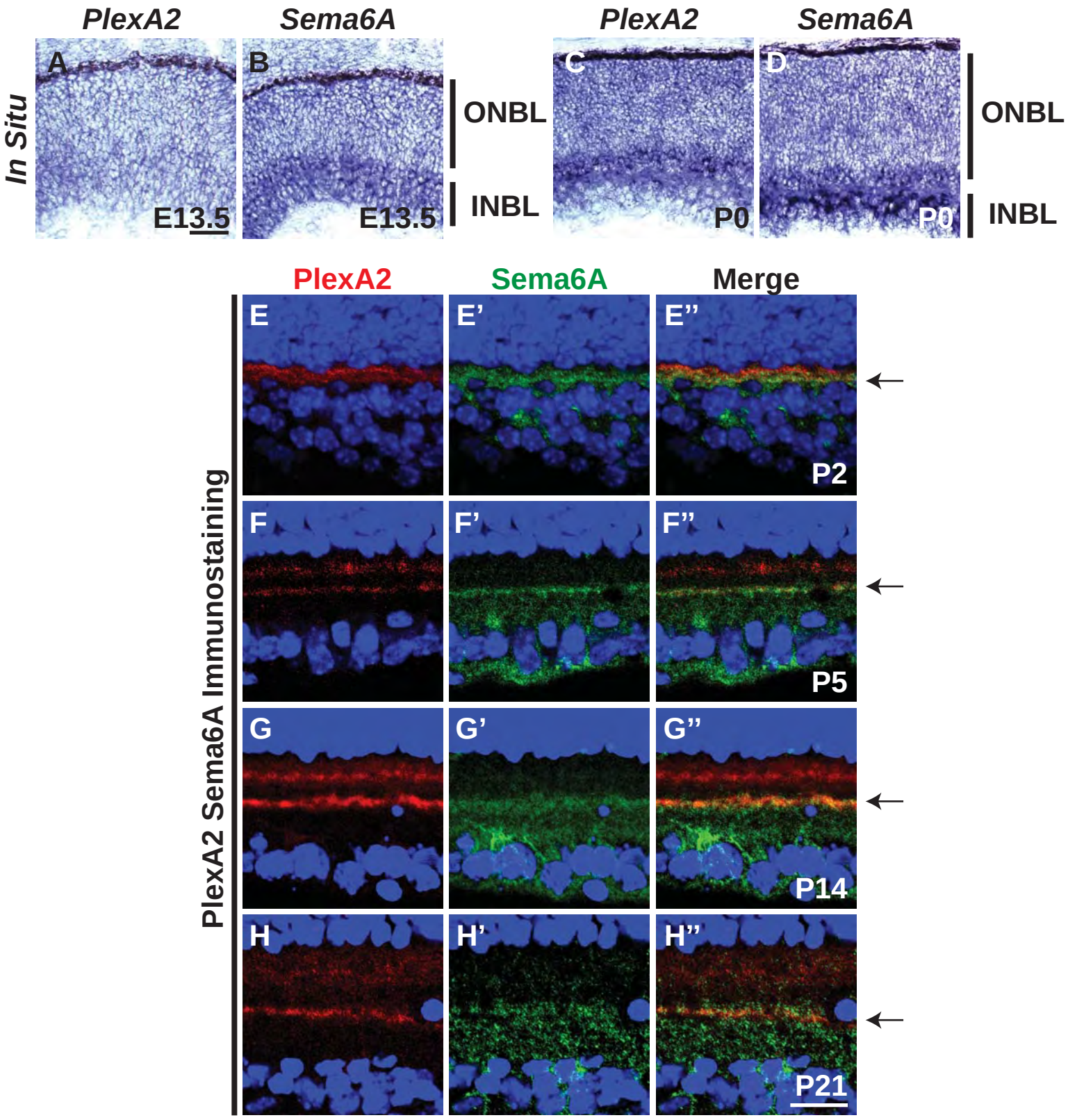
PlexA2
Sema6A
PlexA2
Sema6A
In Situ
A
B
C
D
ONBL
INBL
ONBL
INBL
E13.5
E13.5
P0
P0
PlexA2
Sema6A
Merge
PlexA2 Sema6A Immunostaining
E
E'
E''
F
F'
F''
G
G'
G''
H
H'
H''
P2
P5
P14
P21
ChAT::cre; ROSALSL-Tdtomato
Sema6A
Tdtomato
Merge
I
I'
I''
Cell#1
Cell#2
6A
Td
Merge
Cell#1
Cell#2
J
J'
J''
K
K'
K''

Fig.S1

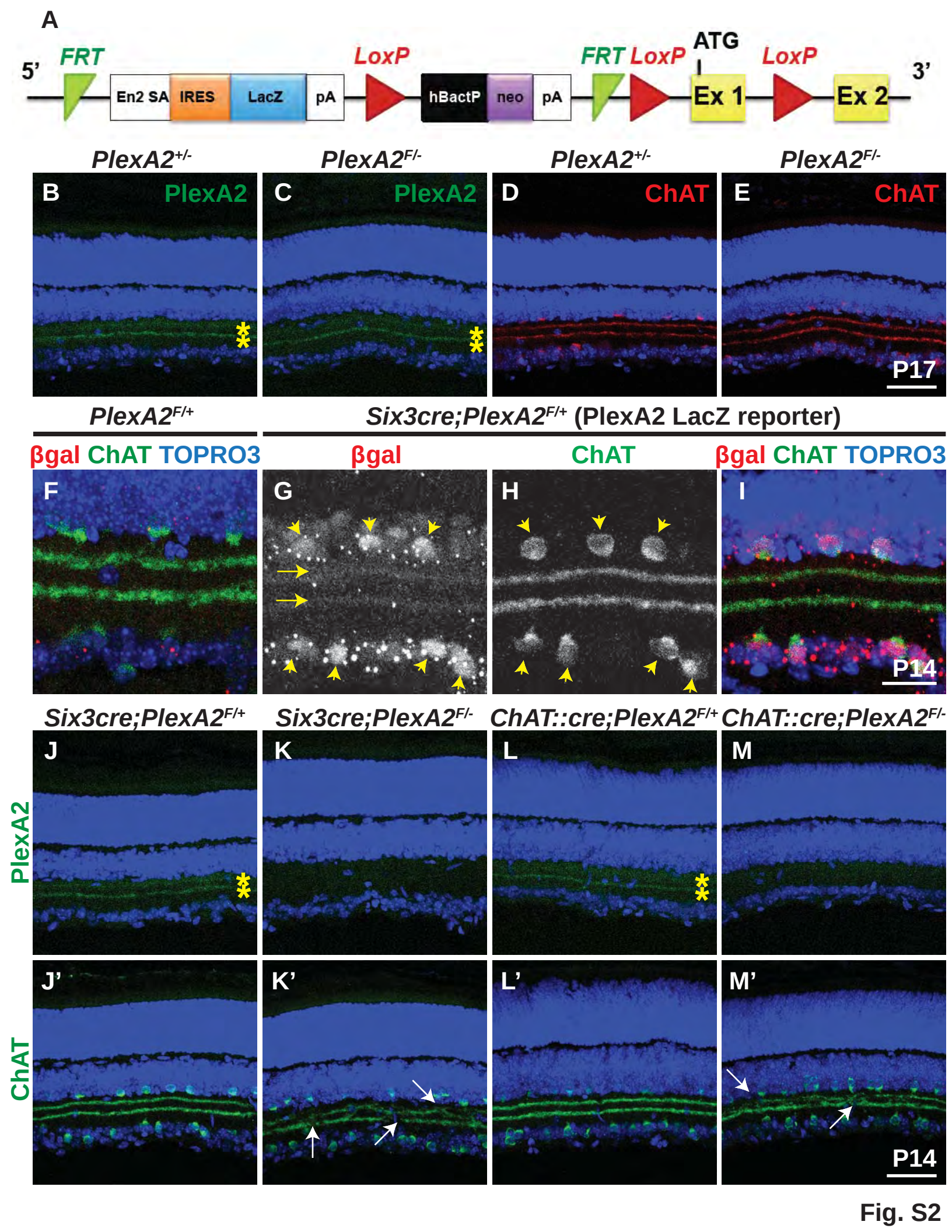
A
5'
FRT
En2 SA
IRES
LacZ
pA
LoxP
hBactP
neo
pA
FRT LoxP
ATG
Ex 1
LoxP
Ex 2
3'
PlexA2+/-
PlexA2F/-
PlexA2+/-
PlexA2F/-
B PlexA2
C PlexA2
D ChAT
E ChAT
P17
PlexA2F/+
Six3cre;PlexA2F/+ (PlexA2 LacZ reporter)
βgal ChAT TOPRO3
βgal
ChAT
βgal ChAT TOPRO3
F
G
H
I
P14
Six3cre;PlexA2F/+
Six3cre;PlexA2F/-
ChAT::cre;PlexA2F/+
ChAT::cre;PlexA2F/-
PlexA2
ChAT
J
K
L
M
J'
K'
L'
M'
P14

Fig. S2

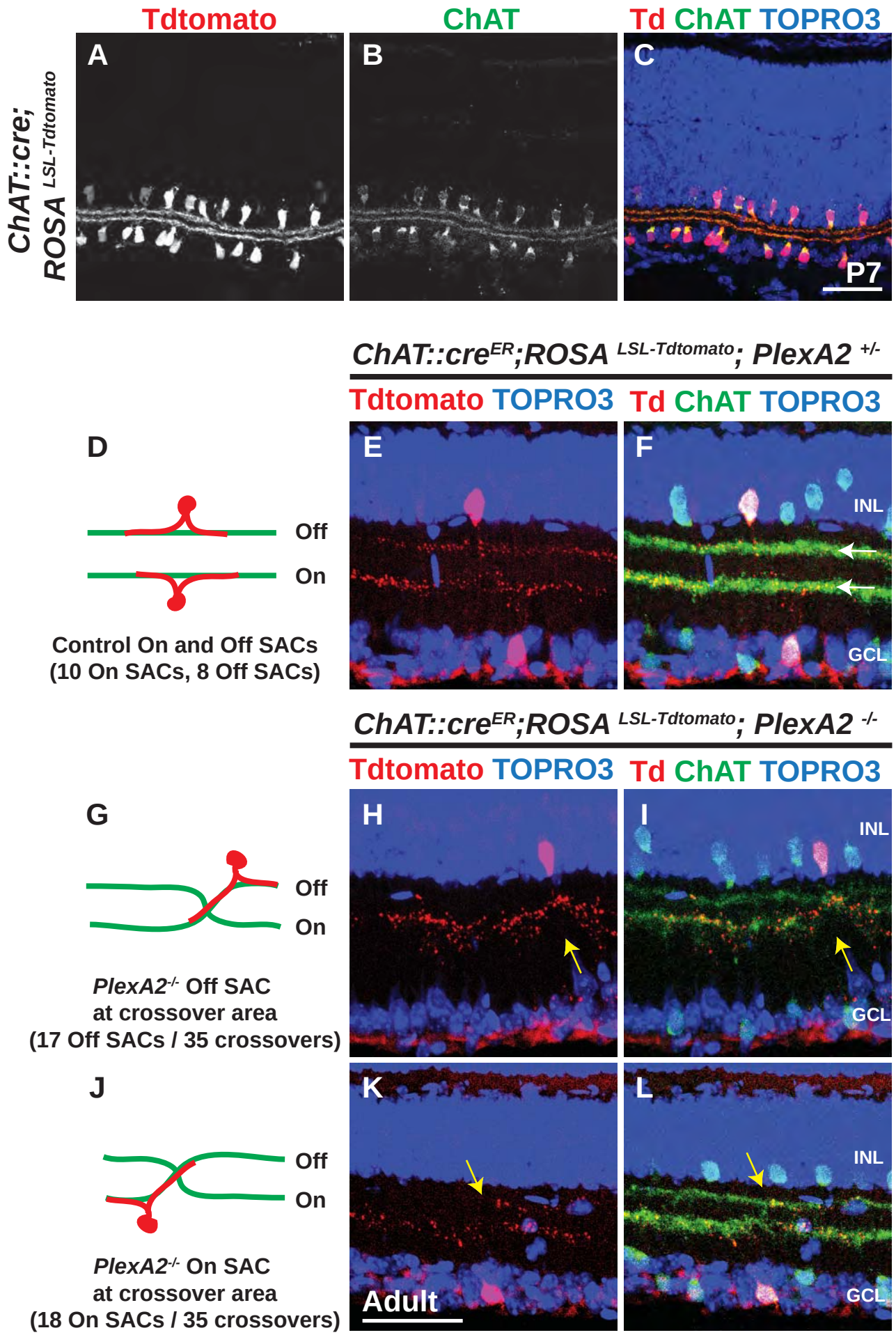
Tdtomato
ChAT
Td ChAT TOPRO3
ChAT::cre; ROSA LSL-Tdtomato
A
B
C
P7
ChAT::creER;ROSA LSL-Tdtomato; PlexA2 +/-
Tdtomato TOPRO3
Td ChAT TOPRO3
D
Off
On
Control On and Off SACs
(10 On SACs, 8 Off SACs)
E
F
INL
GCL
ChAT::creER;ROSA LSL-Tdtomato; PlexA2 -/-
Tdtomato TOPRO3
Td ChAT TOPRO3
G
Off
On
PlexA2-/- Off SAC
at crossover area
(17 Off SACs / 35 crossovers)
H
I
INL
GCL
J
Off
On
PlexA2-/- On SAC
at crossover area
(18 On SACs / 35 crossovers)
K
L
INL
GCL
Adult

Fig. S3

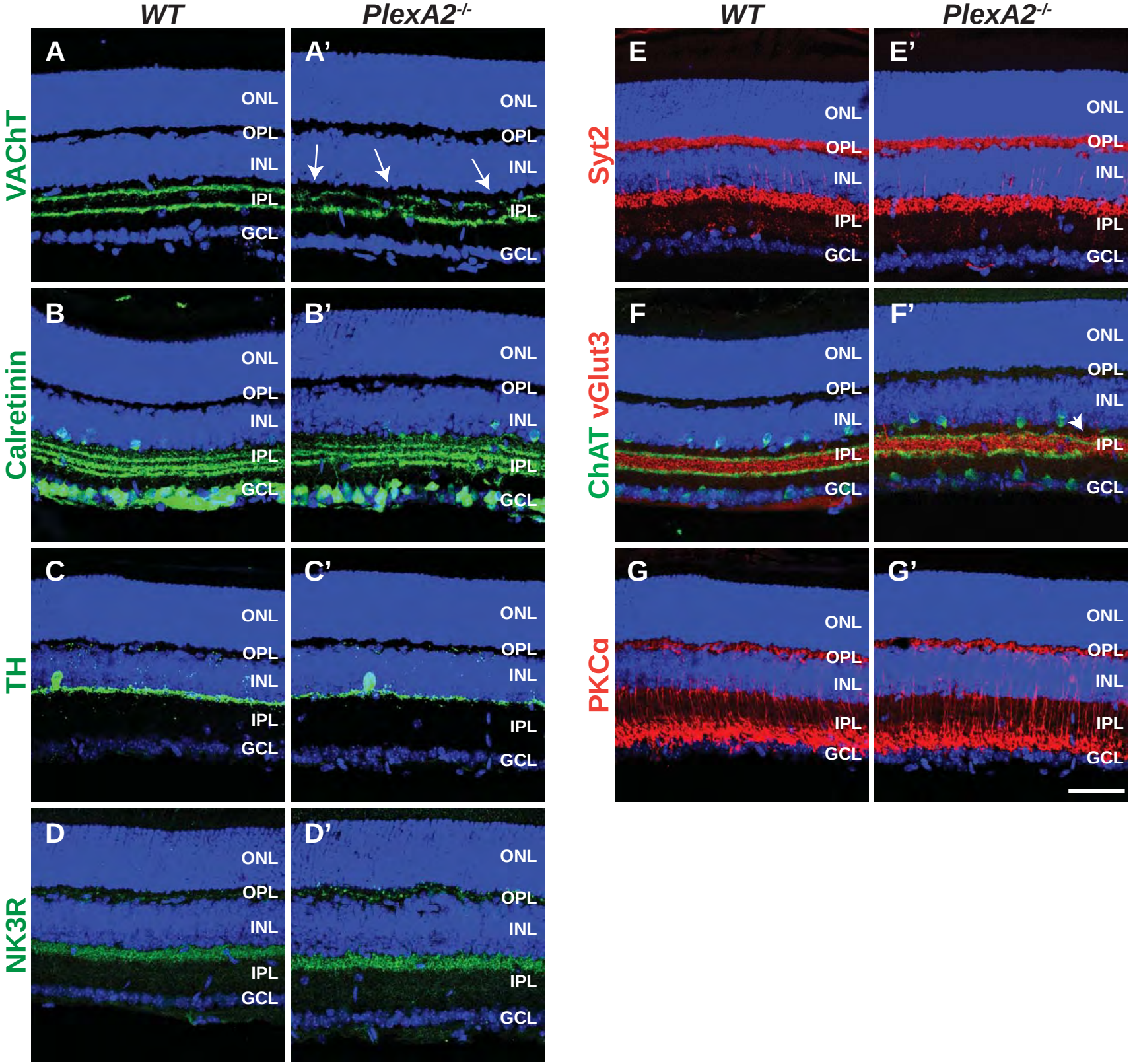
WT
PlexA2-/-
WT
PlexA2-/-
A
A'
E
E'
VAChT
Syt2
B
B'
F
F'
Calretinin
ChAT vGlut3
C
C'
G
G'
TH
PKCα
D
D'
NK3R
ONL
OPL
INL
IPL
GCL

Fig. S4

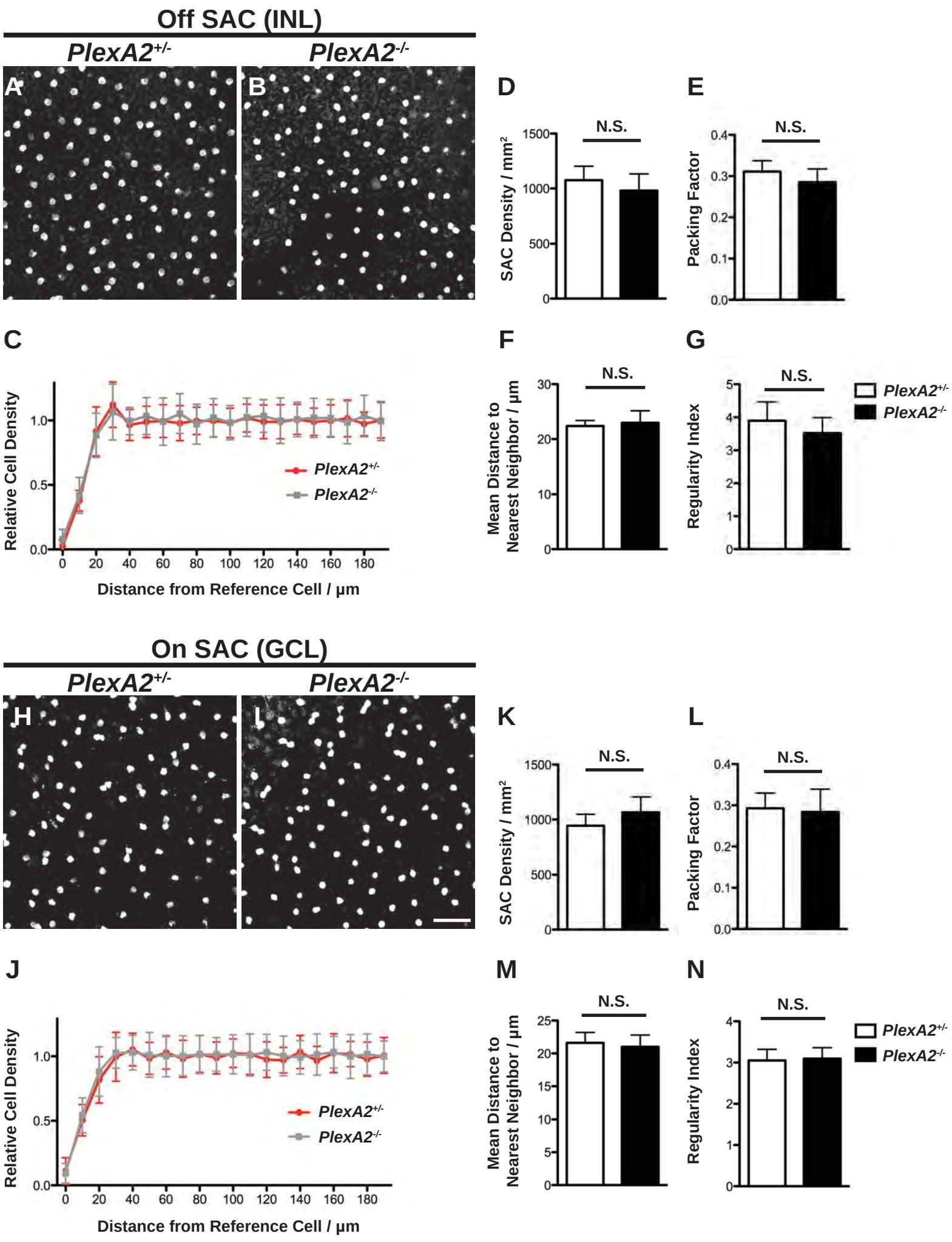
Off SAC (INL)
PlexA2+/-
PlexA2-/-
ChAT
A
B
C
D
E
F
G
N.S.
SAC Density / mm2
Packing Factor
Mean Distance to Nearest Neighbor / µm
Regularity Index
Relative Cell Density
Distance from Reference Cell / µm
On SAC (GCL)
H
I
J
K
L
M
N

Fig. S5

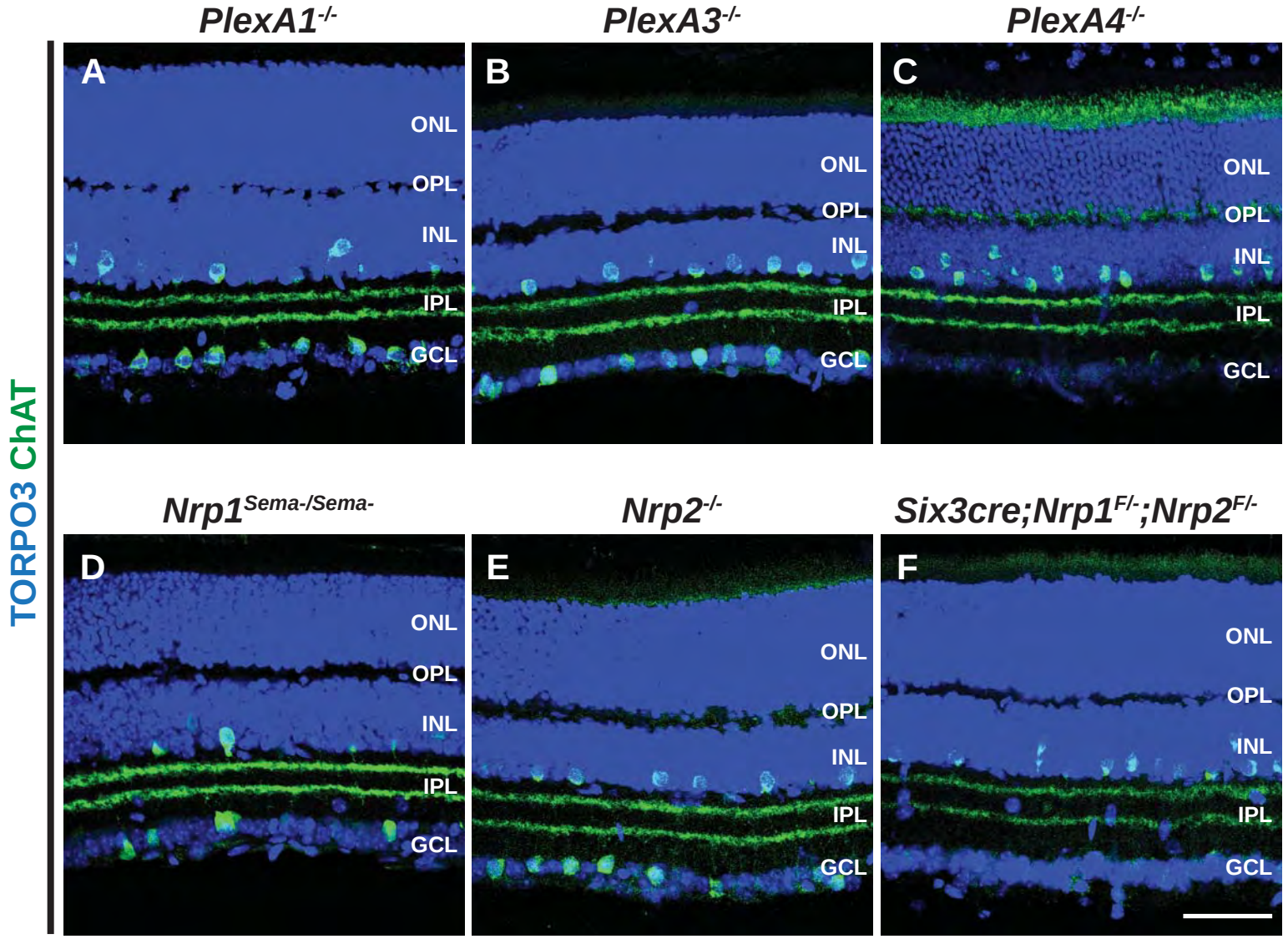
PlexA1-/-
PlexA3-/-
PlexA4-/-
A
B
C
ONL
OPL
INL
IPL
GCL
TORPO3 ChAT
Nrp1Sema-/Sema-
Nrp2-/-
Six3cre;Nrp1F/-;Nrp2F/-
D
E
F

Fig. S6

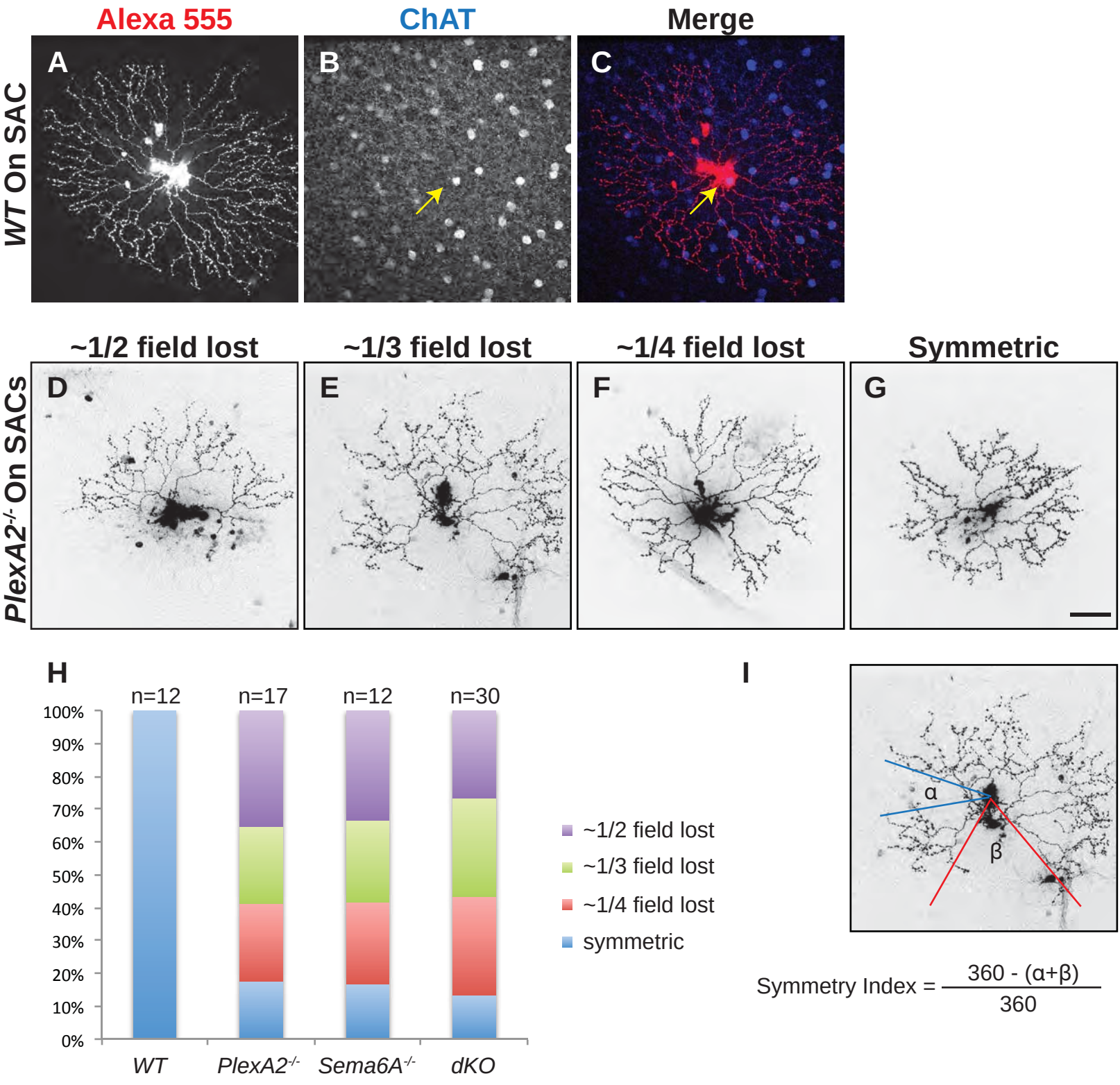
Alexa 555
ChAT
Merge
A
B
C
WT On SAC
~1/2 field lost
~1/3 field lost
~1/4 field lost
Symmetric
D
E
F
G
PlexA2-/- On SACs
H
n=12
n=17
n=12
n=30
100%
90%
80%
70%
60%
50%
40%
30%
20%
10%
0%
WT
PlexA2-/-
Sema6A-/-
dKO
~1/2 field lost
~1/3 field lost
~1/4 field lost
symmetric
I
α
β
Symmetry Index = 360 - (α+β) / 360

Fig. S7

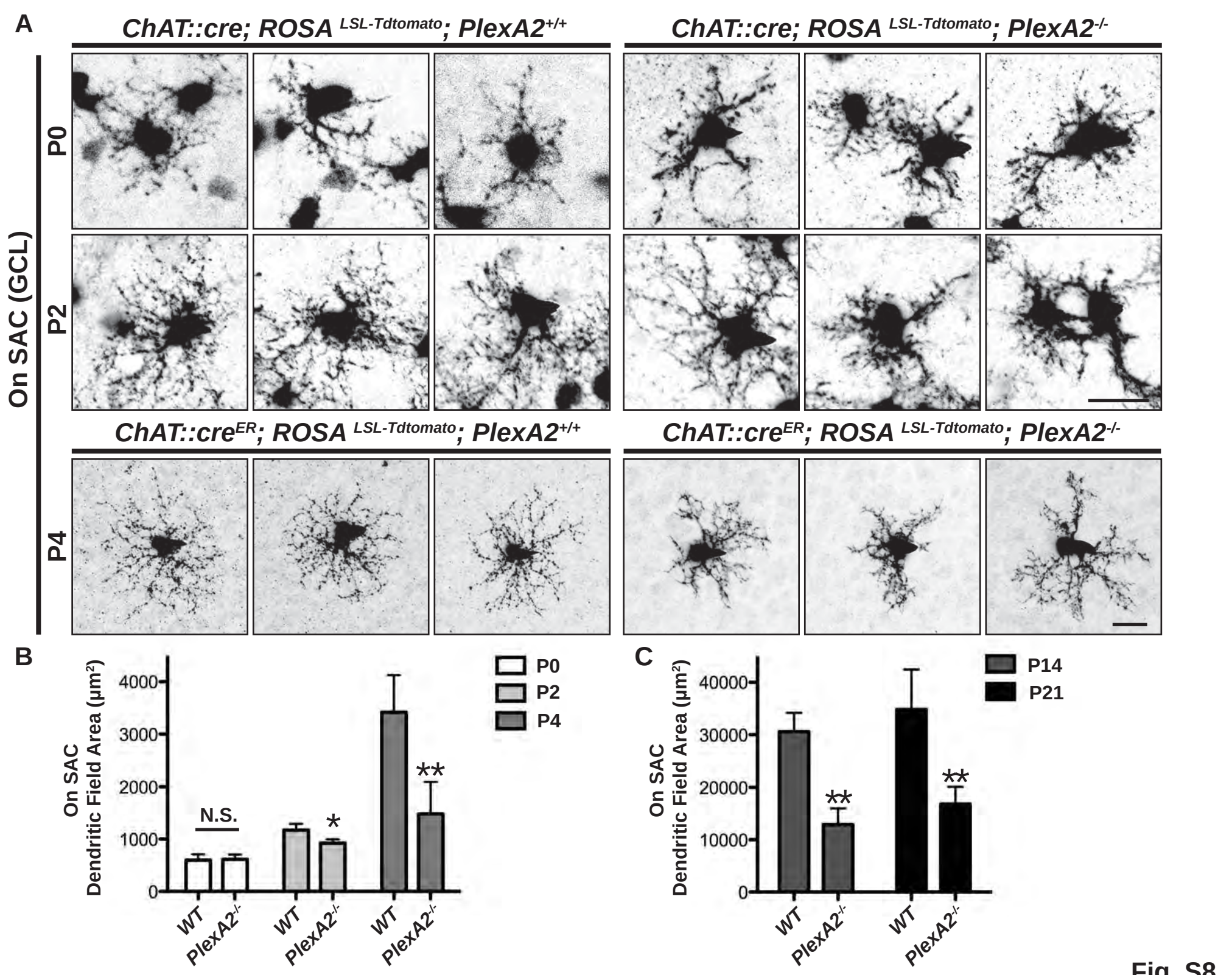
A
ChAT::cre; ROSA LSL-Tdtomato; PlexA2+/+
ChAT::cre; ROSA LSL-Tdtomato; PlexA2-/-
ChAT::creER; ROSA LSL-Tdtomato; PlexA2+/+
ChAT::creER; ROSA LSL-Tdtomato; PlexA2-/-
On SAC (GCL)
P0
P2
P4
B
On SAC Dendritic Field Area (μm²)
4000
3000
2000
1000
0
N.S.
*
**
P0
P2
P4
WT
PlexA2-/-
C
On SAC Dendritic Field Area (μm²)
40000
30000
20000
10000
0
**
**
P14
P21
WT
PlexA2-/-

Fig. S8

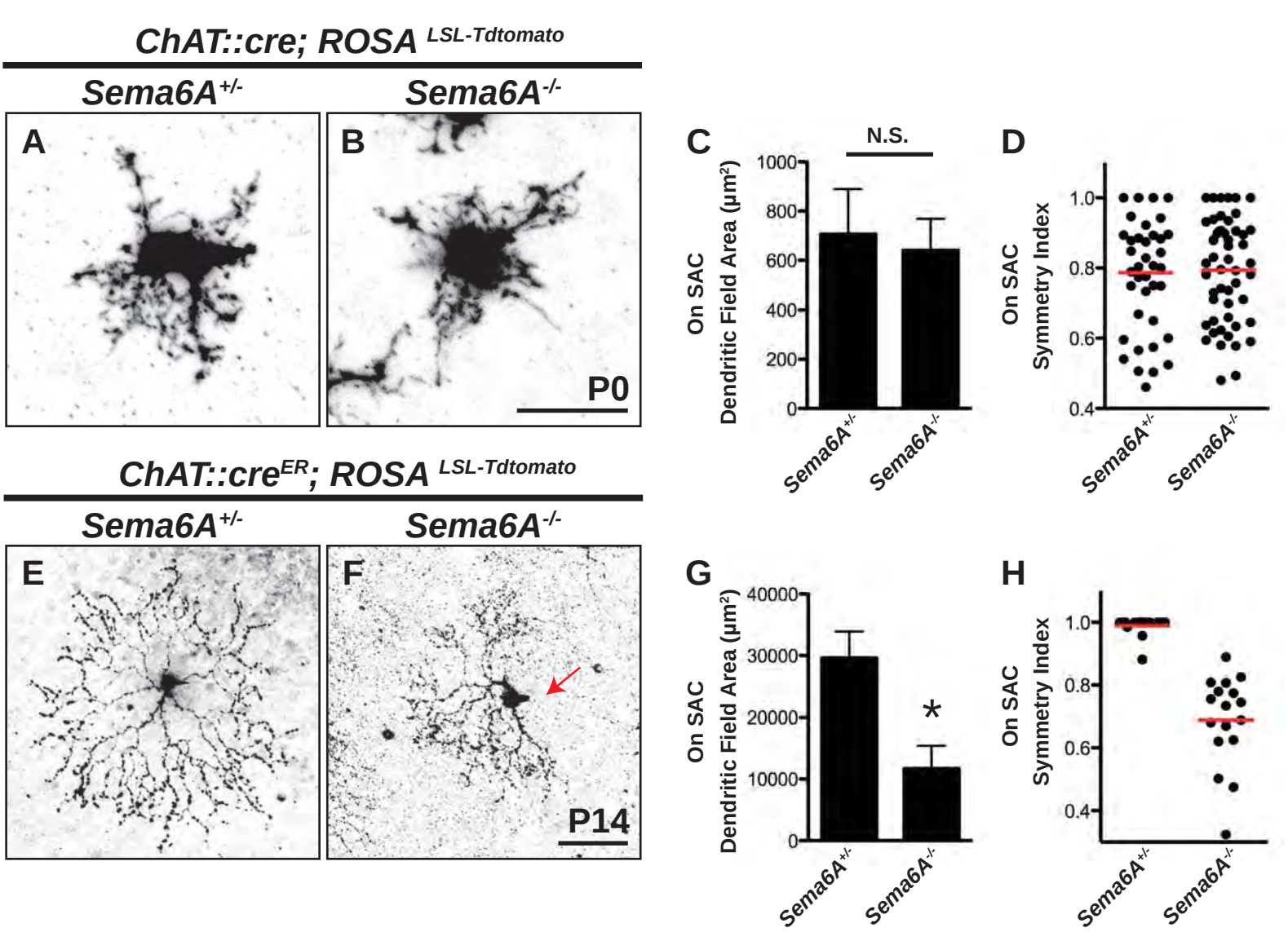
ChAT::cre; ROSA LSL-Tdtomato
Sema6A+/-
Sema6A-/-
A
B
P0
C
N.S.
On SAC Dendritic Field Area (µm²)
1000
800
600
400
200
0
Sema6A+/-
Sema6A-/-
D
On SAC Symmetry Index
1.0
0.8
0.6
0.4
Sema6A+/-
Sema6A-/-
ChAT::creER; ROSA LSL-Tdtomato
Sema6A+/-
Sema6A-/-
E
F
P14
G
On SAC Dendritic Field Area (µm²)
40000
30000
20000
10000
0
*
Sema6A+/-
Sema6A-/-
H
On SAC Symmetry Index
1.0
0.8
0.6
0.4
Sema6A+/-
Sema6A-/-

Fig. S9

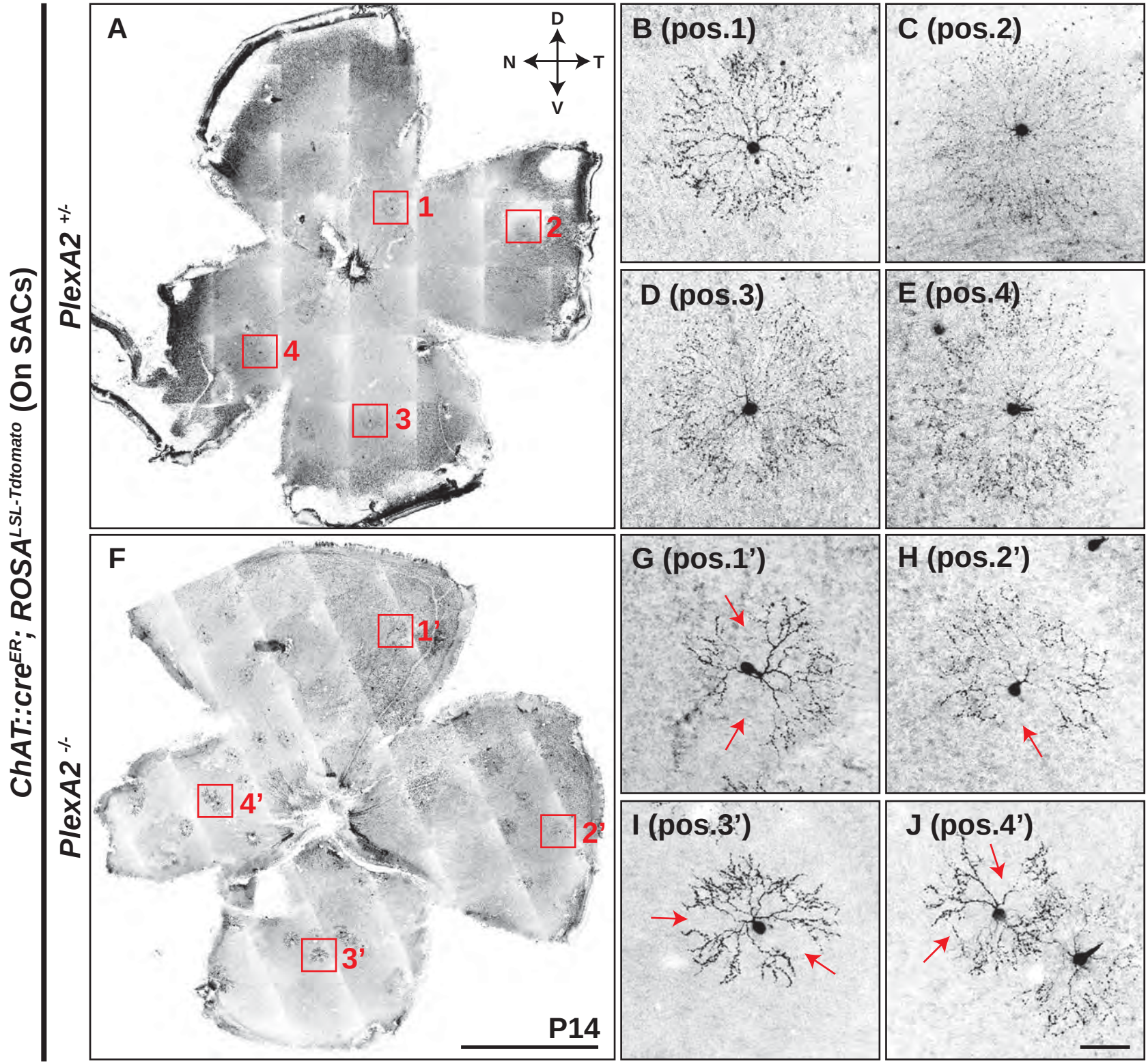
ChAT::cre^ER; ROSA^LSL-Tdtomato (On SACs)
PlexA2 +/-
PlexA2 -/-
A
D
N
T
V
1
2
3
4
B (pos.1)
C (pos.2)
D (pos.3)
E (pos.4)
F
1'
2'
3'
4'
P14
G (pos.1')
H (pos.2')
I (pos.3')
J (pos.4')

Fig. S10

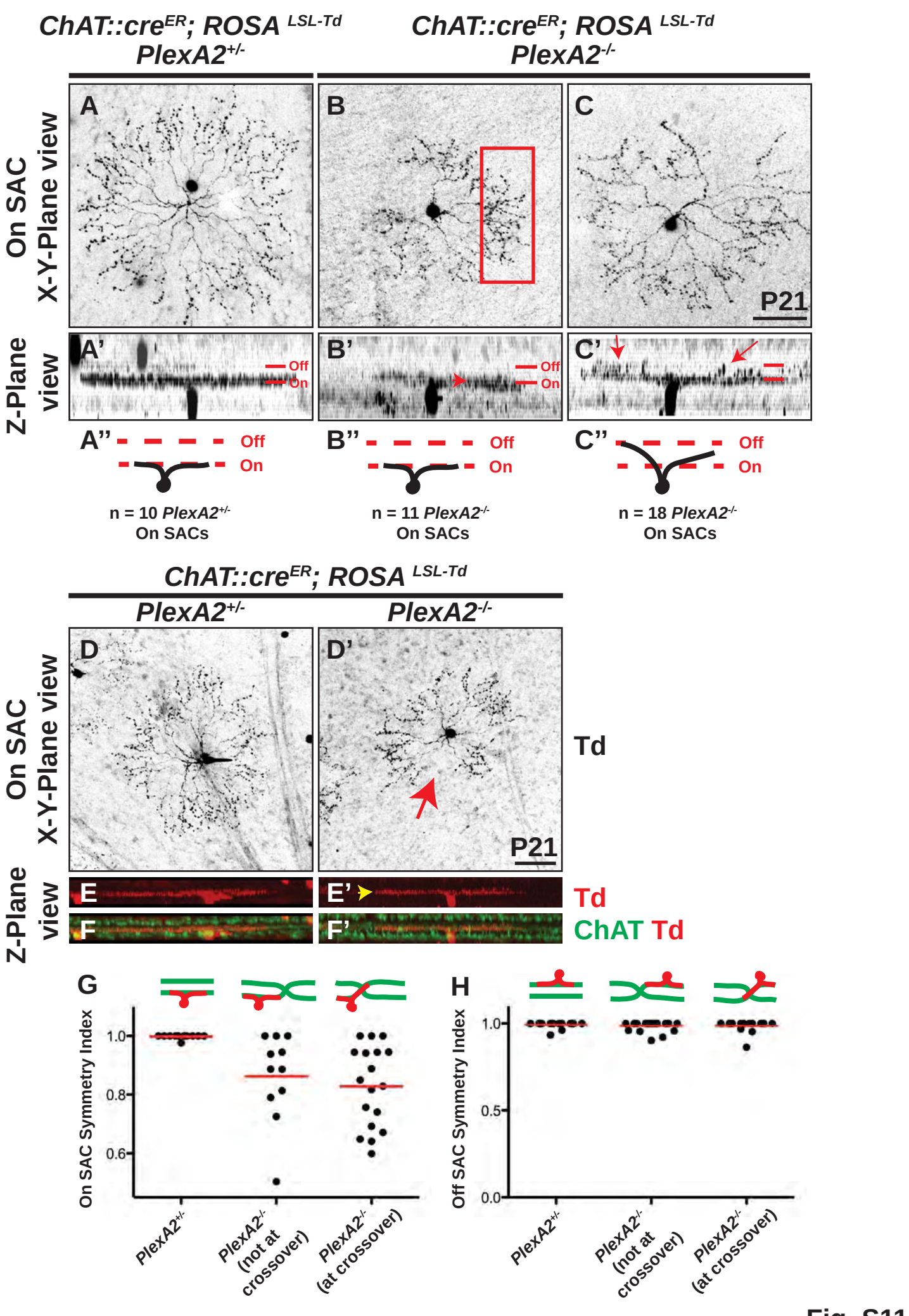
ChAT::cre^ER; ROSA LSL-Td
PlexA2+/-
ChAT::cre^ER; ROSA LSL-Td
PlexA2-/-
On SAC X-Y-Plane view
Z-Plane view
A
B
C
P21
A'
B'
C'
Off
On
A''
B''
C''
n = 10 PlexA2+/- On SACs
n = 11 PlexA2-/- On SACs
n = 18 PlexA2-/- On SACs
ChAT::cre^ER; ROSA LSL-Td
PlexA2+/-
PlexA2-/-
D
D'
P21
Td
E
E'
F
F'
Td
ChAT Td
G
On SAC Symmetry Index
1.0
0.8
0.6
PlexA2+/-
PlexA2-/- (not at crossover)
PlexA2-/- (at crossover)
H
Off SAC Symmetry Index
1.0
0.5
0.0
PlexA2+/-
PlexA2-/- (not at crossover)
PlexA2-/- (at crossover)

Fig. S11

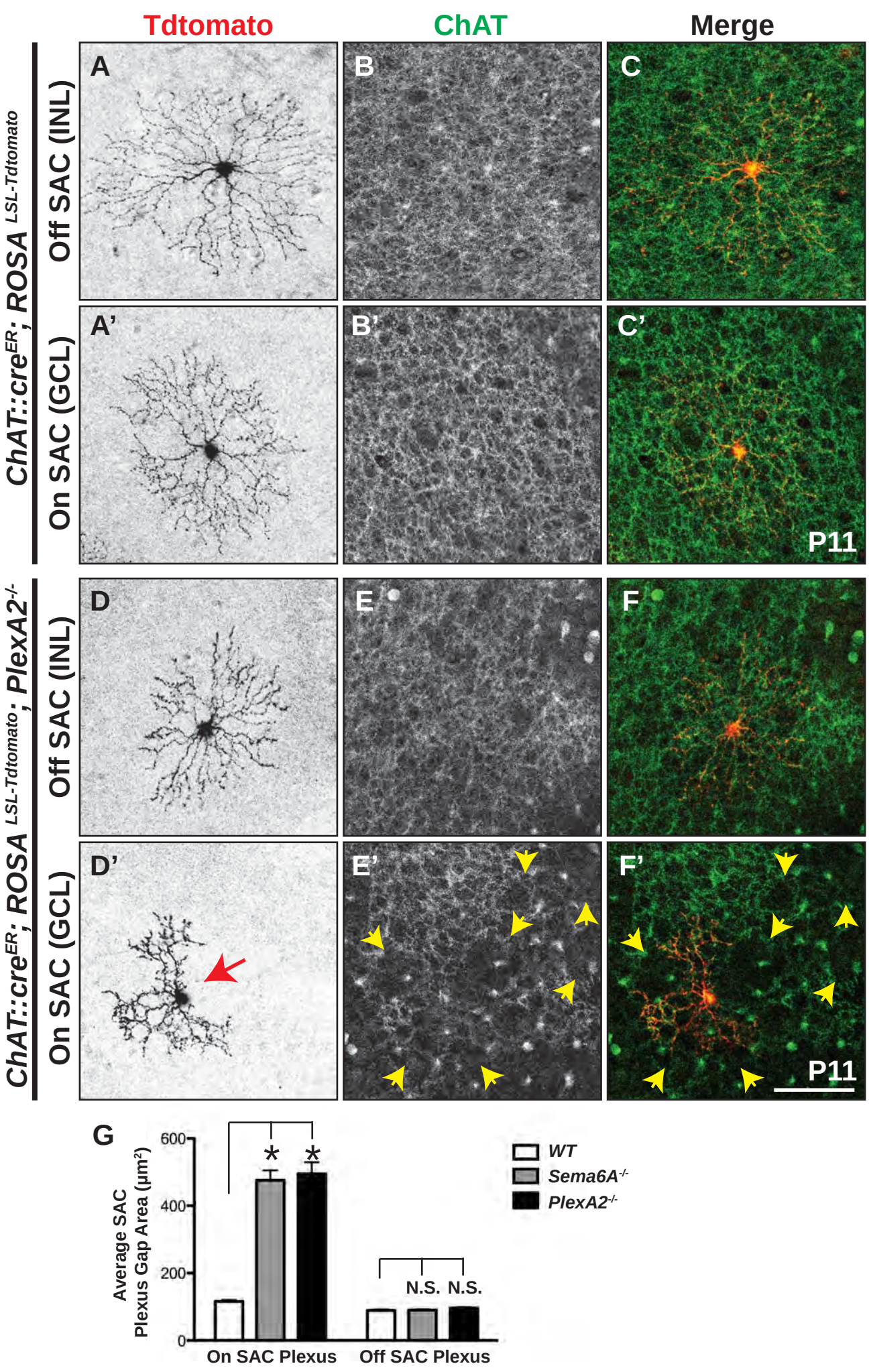
Tdtomato
ChAT
Merge
ChAT::cre^ER; ROSA LSL-Tdtomato
Off SAC (INL)
On SAC (GCL)
A
B
C
A'
B'
C'
P11
ChAT::cre^ER; ROSA LSL-Tdtomato; PlexA2-/-
Off SAC (INL)
On SAC (GCL)
D
E
F
D'
E'
F'
P11
G
Average SAC Plexus Gap Area (µm²)
600
400
200
0
*
*
N.S.
N.S.
On SAC Plexus
Off SAC Plexus
WT
Sema6A-/-
PlexA2-/-

Fig. S12

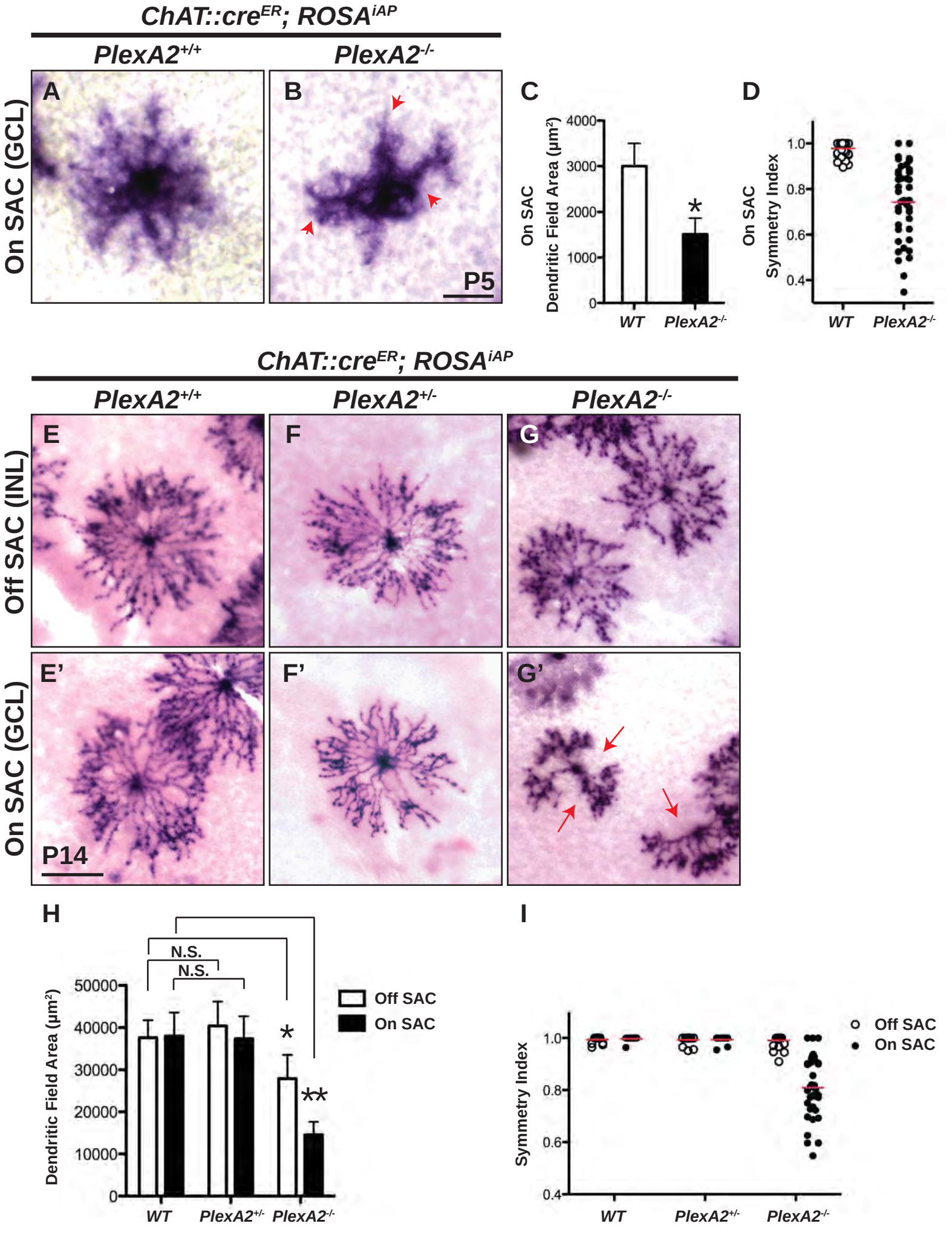
ChAT::cre^ER; ROSA^iAP
PlexA2+/+
PlexA2-/-
On SAC (GCL)
A
B
P5
C
On SAC Dendritic Field Area (μm²)
4000
3000
2000
1000
0
*
WT
PlexA2-/-
D
On SAC Symmetry Index
1.0
0.8
0.6
0.4
WT
PlexA2-/-
ChAT::cre^ER; ROSA^iAP
PlexA2+/+
PlexA2+/-
PlexA2-/-
Off SAC (INL)
On SAC (GCL)
E
F
G
E'
F'
G'
P14
H
N.S.
N.S.
Dendritic Field Area (μm²)
50000
40000
30000
20000
10000
0
*
**
Off SAC
On SAC
WT
PlexA2+/-
PlexA2-/-
I
Symmetry Index
1.0
0.8
0.6
0.4
Off SAC
On SAC
WT
PlexA2+/-
PlexA2-/-

Fig. S13

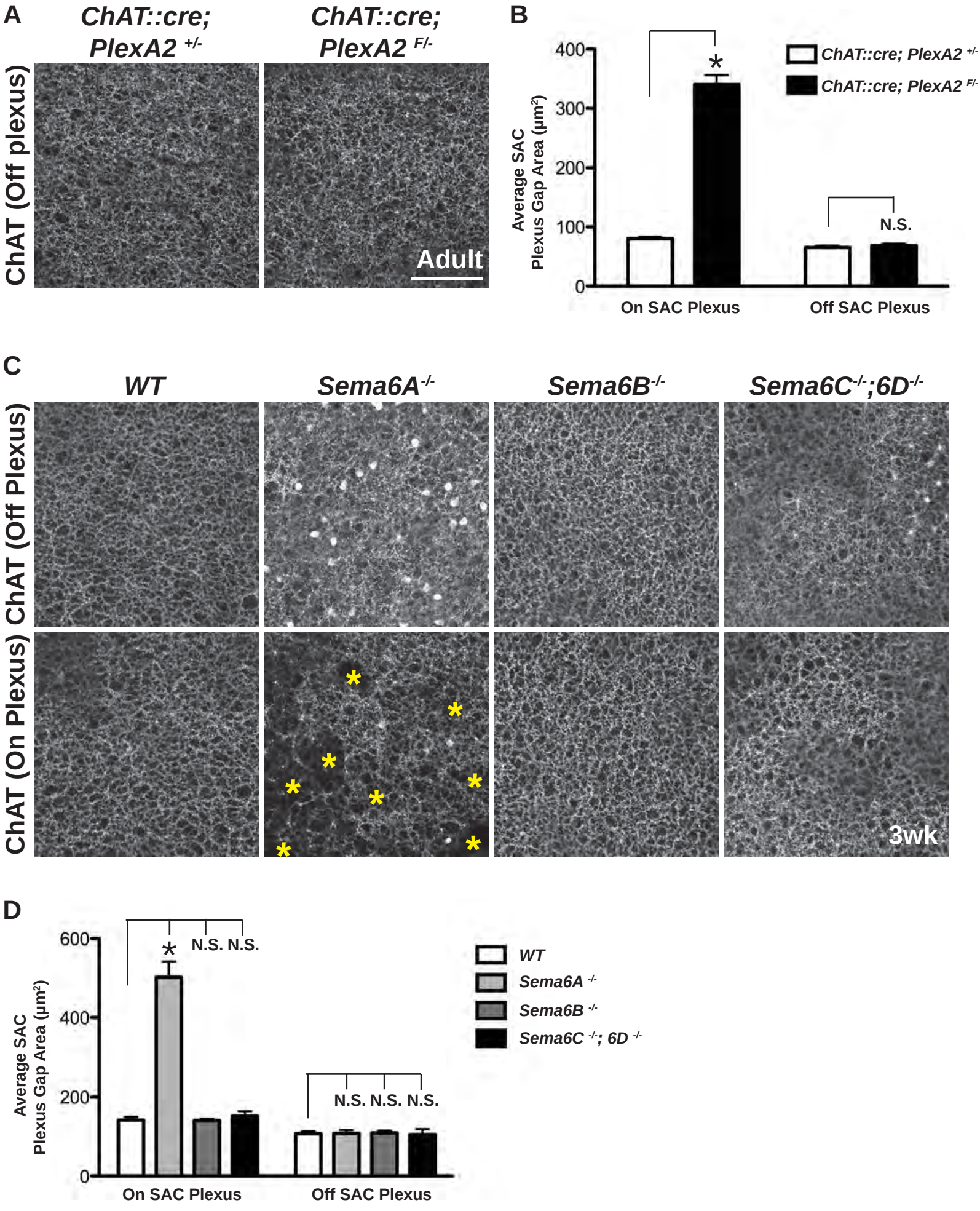
A
ChAT::cre; PlexA2 +/-
ChAT::cre; PlexA2 F/-
ChAT (Off plexus)
Adult
B
Average SAC Plexus Gap Area (µm²)
400
300
200
100
0
*
N.S.
ChAT::cre; PlexA2 +/-
ChAT::cre; PlexA2 F/-
On SAC Plexus
Off SAC Plexus
C
WT
Sema6A-/-
Sema6B-/-
Sema6C-/-;6D-/-
ChAT (Off Plexus)
ChAT (On Plexus)
3wk
D
Average SAC Plexus Gap Area (µm²)
600
400
200
0
*
N.S. N.S.
N.S. N.S. N.S.
On SAC Plexus
Off SAC Plexus
WT
Sema6A -/-
Sema6B -/-
Sema6C -/-; 6D -/-

Fig. S14

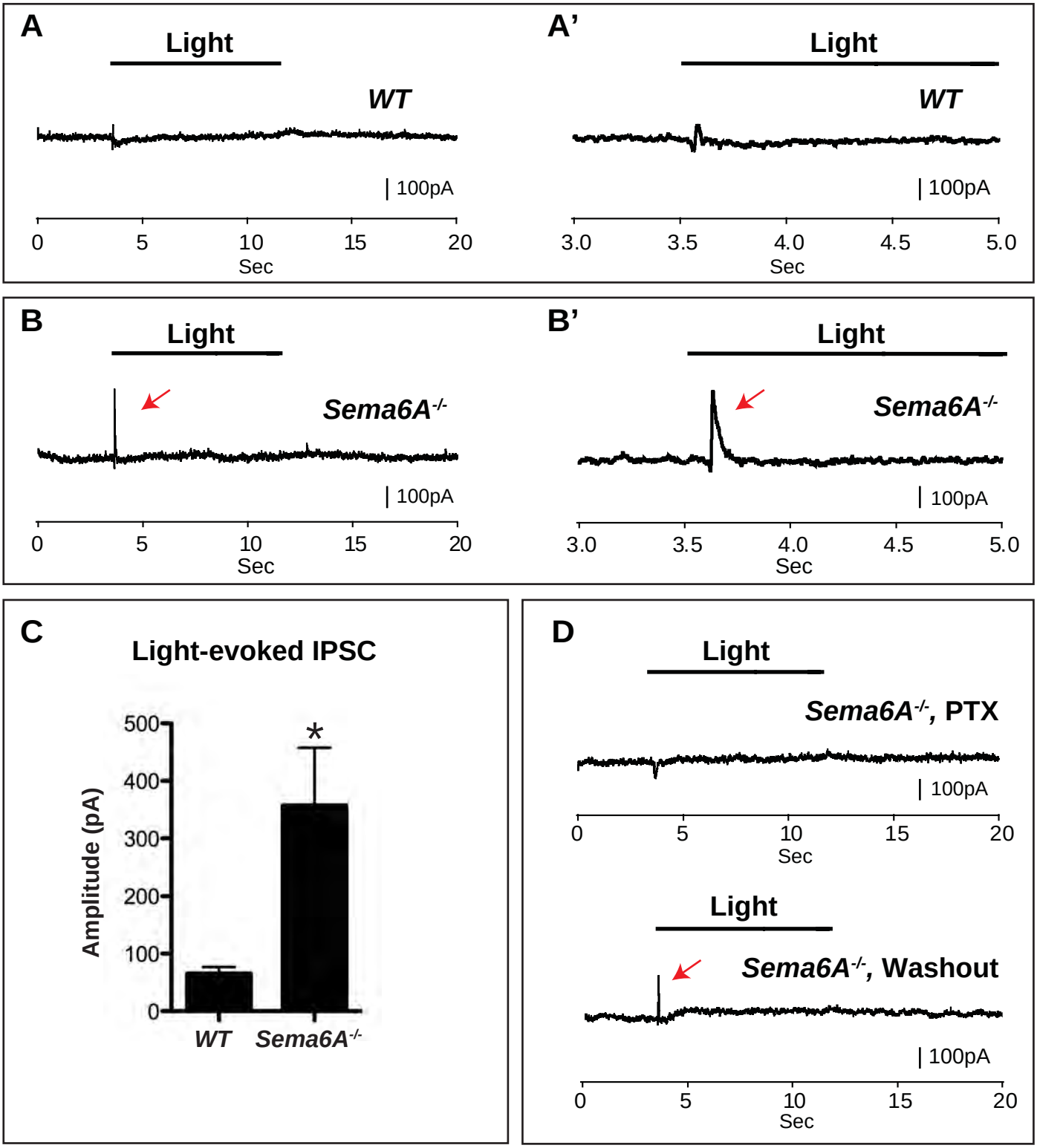
A
Light
WT
100pA
0
5
10
15
20
Sec
A'
Light
WT
100pA
3.0
3.5
4.0
4.5
5.0
Sec
B
Light
Sema6A-/-
100pA
0
5
10
15
20
Sec
B'
Light
Sema6A-/-
100pA
3.0
3.5
4.0
4.5
5.0
Sec
C
Light-evoked IPSC
Amplitude (pA)
500
400
300
200
100
0
*
WT
Sema6A-/-
D
Light
Sema6A-/-, PTX
100pA
0
5
10
15
20
Sec
Light
Sema6A-/-, Washout
100pA
0
5
10
15
20
Sec

Fig. S15

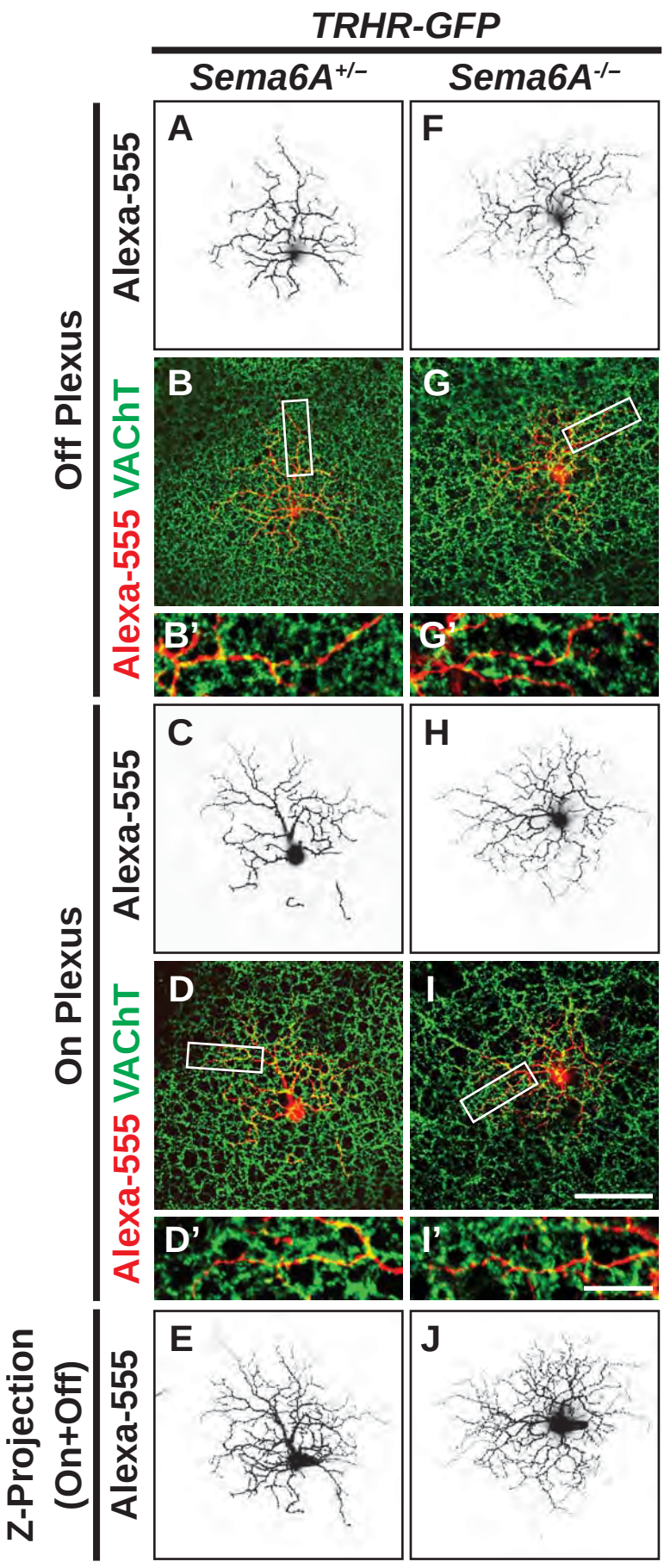
TRHR-GFP
Sema6A+/–
Sema6A-/–
Off Plexus
Alexa-555
Alexa-555 VAChT
On Plexus
Alexa-555
Alexa-555 VAChT
Z-Projection (On+Off)
Alexa-555
A
F
B
G
B'
G'
C
H
D
I
D'
I'
E
J

Fig. S16

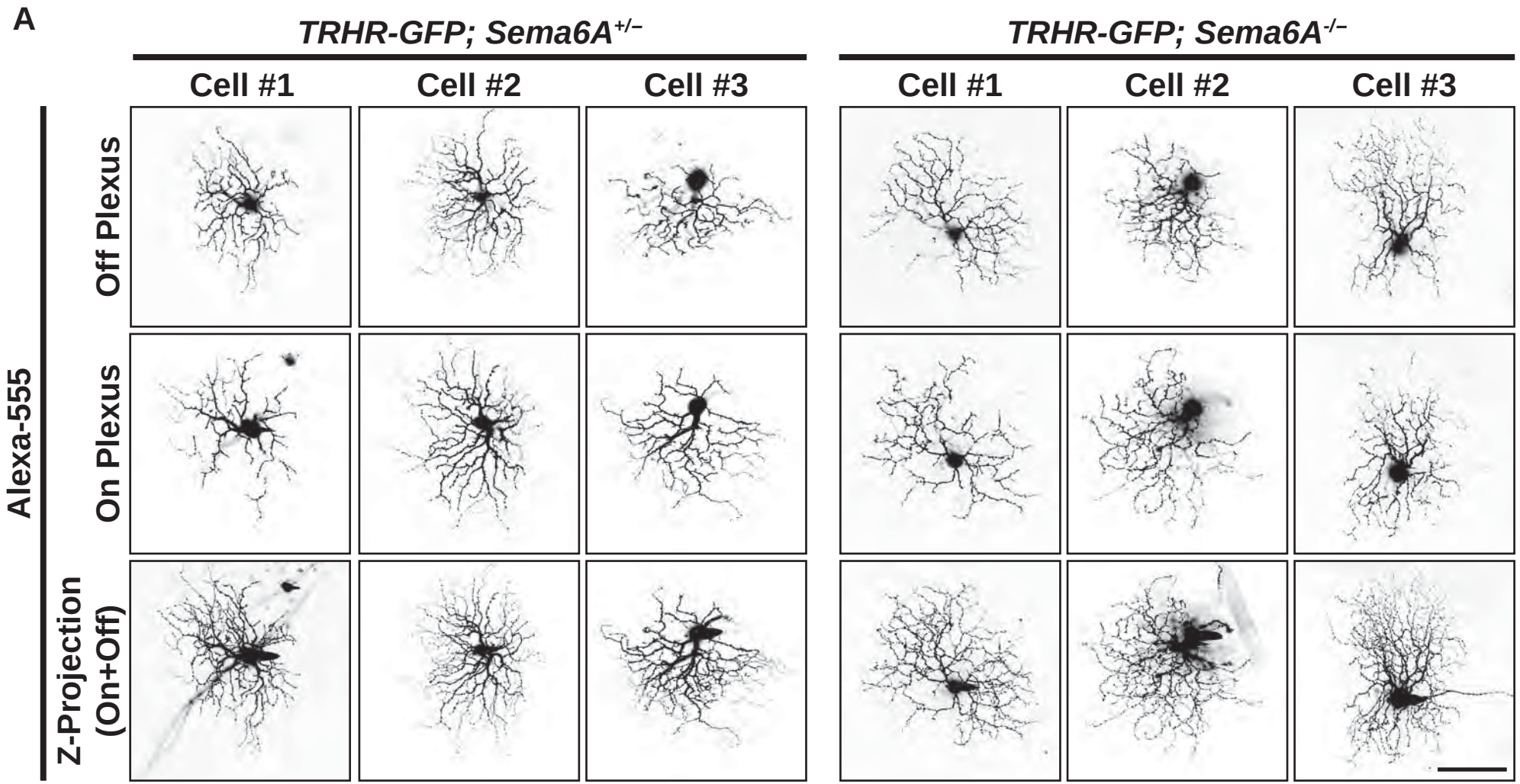
A
TRHR-GFP; Sema6A+/–
TRHR-GFP; Sema6A-/–
Cell #1
Cell #2
Cell #3
Cell #1
Cell #2
Cell #3
Alexa-555
Off Plexus
On Plexus
Z-Projection (On+Off)

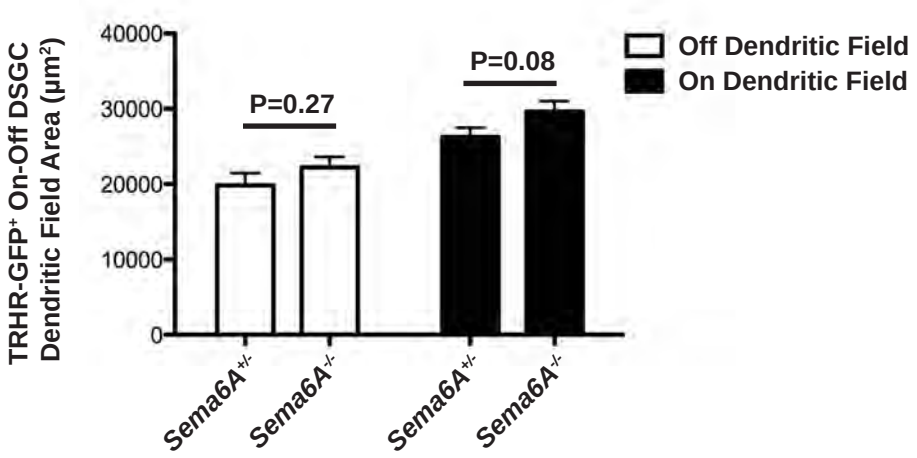
B
TRHR-GFP+ On-Off DSGC Dendritic Field Area (µm²)
40000
30000
20000
10000
0
P=0.27
P=0.08
Off Dendritic Field
On Dendritic Field
Sema6A+/-
Sema6A-/-
Sema6A+/-
Sema6A-/-

Fig. S17